6-27-1995

Simulation of Electron Emission from Beryllium Under Electron and Ion Bombardments

Kaoru Ohya
The University of Tokushima

Jun Kawata
Takuma National College of Technology

Utah State University
MERRILL-CAZIER LIBRARY

SIMULATION OF ELECTRON EMISSION FROM BERYLLIUM UNDER ELECTRON AND ION BOMBARDMENTS

Kaoru Ohya[*] and Jun Kawata[1]

Department of Electrical and Electronic Engg., Fac. Engg., The University of Tokushima, Tokushima 770, Japan
[1]Department of Information Engineering, Takuma National College of Technology, Takuma, Kagawa 769-11, Japan

Abstract

A Monte Carlo simulation model of particle-induced electron emission from beryllium, a candidate material for use on the wall in thermonuclear fusion devices, is developed. Comparative studies between secondary electron emission by electron bombardment and kinetic electron emission by proton bombardment reveal some interesting similarities and differences. The kinetic emission of electrons under heavy-ion bombardment is simulated as well for analyzing the effect of the initial charge state and mass of projectile ions on the kinetic emission. Furthermore, the model is applied to bowl-and-ripple structures for the study of surface roughness effects on the energy and angular distributions of secondary electrons, as well as of the secondary electron yield of beryllium under electron bombardment.

Key Words: Secondary electron emission, kinetic electron emission, beryllium, Monte Carlo simulation, surface roughness, plasma-surface interaction, primary electron, proton, heavy-ion, multi-charged ion.

[*]Address for correspondence:
Kaoru Ohya,
Department of Electrical and Electronic Engineering,
Faculty of Engineering,
The University of Tokushima,
Tokushima 770,
Japan

Telephone number: +81 886 56 7444
FAX number: +81 886 54 9632
E-mail: ohya@ee.tokushima-u.ac.jp

Introduction

For more than 20 years, low atomic number (Z) materials, such as graphite, have been used as plasma-facing materials (PFM) in magnetic confinement fusion devices [66]. The advantages that graphite possesses over stainless steel or titanium, which had been used previously, are: its lower radiation cooling rate, very high sublimation temperature, good resistance to thermal shocks, and the absence of the surface instability caused by melting. However, the hydrogen release during discharges, the fuel dilution, and the carbon bloom have presented serious obstacles to a further development of fusion research. Although very high Z metals, such as molybdenum or tungsten, resolve some of these problems [69], these refractory materials cause unacceptable plasma cooling by impurity accumulation and resultant radiation unless the edge plasma temperature can be held very low (less than several tens of eV).

Particle-induced electron emission from the PFM is a plasma-surface interaction process of considerable importance for impurity production due to sputtering of the PFM [32]. Low-energy electrons emitted from the surface reduce the edge plasma temperature [49]; also, through reducing the plasma sheath potential, they lower the energy of ions incident on the PFM, and hence, the sputtering yield and impurity production [16]. The existing experimental data on the particle-induced electron emission are less than those for particle backscattering and sputtering; furthermore, the electron yield and the energy and angular distributions of emitted electrons are very sensitive to surface contamination due to surface conditions, e.g., changes in the work function of the surface. PFM surfaces exhibit a pronounced macroscopic roughness, mostly due to the production process, with microscopic (atomic scale) roughness superimposed. Plasma-surface interaction processes induce various morphological and microstructural property changes in the PFM. During exposure to plasmas, therefore, surface roughness is modified mainly due to sputtering and redeposition, depending on the energy, angle and dose of incident particle flux, and the composition of the PFM.

Table of Symbols

E	instantaneous energy of projectile particle, recoiling solid atoms and secondary (kinetic) electrons in a solid
E_F	Fermi energy of the free-electron gas
E_i	first ionization energy of inner-shell electrons
E_m	maximum energy of primary electrons excited for ion impact
E_p	projectile energy
E_s	energy of secondary (kinetic) electrons emitted in vacuum
E_{th}	threshold energy for kinetic electron emission
E_τ	fitting parameter in $\tau(E)$
$G(k)$	correction term for Lindhard's polarizability
H	depth of depression in bowl-and-ripple structured surfaces (Fig. 4)
L	free flight path for an elastic collision of ions (recoiling solid atoms) in a solid
m_e	electron mass
m_p	mass of projectile ions
m_t	mass of target solid atoms
n	number of electrons emitted per impinging projectile
N	atomic density of solid
P	impact parameter in an elastic collision between a projectile ion (recoiling solid atom) and an ionic core in a solid
$P(k,\omega)$	Lindhard's polarizability
$P_n(\gamma)$	Poisson distribution for emission of n electrons with mean value γ
q	initial charge state of projectile ion
q_c	cut-off wave number of the bulk plasmon dispersion relation
R	maximum range of a primary electron in a solid
V_F	Fermi velocity of the free-electron gas
v_p	velocity of a projectile ion
v_{th}	threshold velocity for kinetic electron emission
W	width of depression in bowl-and-ripple structured surfaces (Fig. 4)
W_n	individual probability for emission of n = 0, 1, 2,.. electrons emitted per impinging projectile
x,y,z	each axis of coordinate defined for model of bowl-and-ripple structured surfaces (Fig. 4)
Z	atomic number of material
γ	kinetic electron yield
δ	true secondary electron yield ($\leq$ 50 eV)
ΔE	energy loss due to inelastic collisions of a moving particle in a solid
$\epsilon(k,\omega)$	wave number (k) and frequency (ω) dependent dielectric function of the free-electron gas
η	electron backscattering coefficient ($>$ 50 eV)
θ	polar emission angle of electrons measured from surface normal (z-axis in Fig. 4)
Θ	scattering angle in an elastic collision of a moving particle in center-of-mass system
σ	total electron yield ($= \delta + \eta$)
$\tau(E)$	energy-dependent screening parameter in the screened Rutherford elastic cross-section
ϕ	incident angle of a projectile (an electron or ion) measured from surface normal (z-axis in Fig. 4)
Φ	work function
ω_p	plasma frequency of the free-electron gas

The effect of the structured surfaces on sputtering and ion backscattering has been calculated and discussed extensively, earlier by Littmark and Hofer [48], and recently by other workers [22, 38, 58, 64, 78, 80], who elucidated its importance in plasma-surface interactions. Such a surface structure and its modifications can change the electron yield as well as the energy and angular distributions of emitted electrons.

Recently, beryllium has been proposed as an alternative to graphite [71]. It has an obvious advantage due to its lower atomic number than carbon, which results in lower radiation cooling of plasma by the sputtered atoms, while physical sputtering yields are very similar to graphite. Beryllium is a simple, nearly-free-electron metal, similar to aluminum, which has become a standard material for use in computer simulations of secondary electron emission for ease of comparison with existing experimental data [57]. For secondary electron emission induced by electron bombardment, there are many computer simulations which may make up for the lack of experimental data; thus, the Monte Carlo technique and theoretical treatment of the simulations can be extended to calculations for beryllium. Electron emission induced by ion bombardment is attributed to kinetic emission from the material similar to electron-induced electron emission and potential emission at a surface arising from Auger neutralization or resonant neutralizations (followed by Auger de-excitation and autoionization) of the projectile [31]. Clearly, for singly charged ions, the dominant emission process will be kinetic emission, except at very low energies. Although electron emission by potential emission occurs by impact of all

332
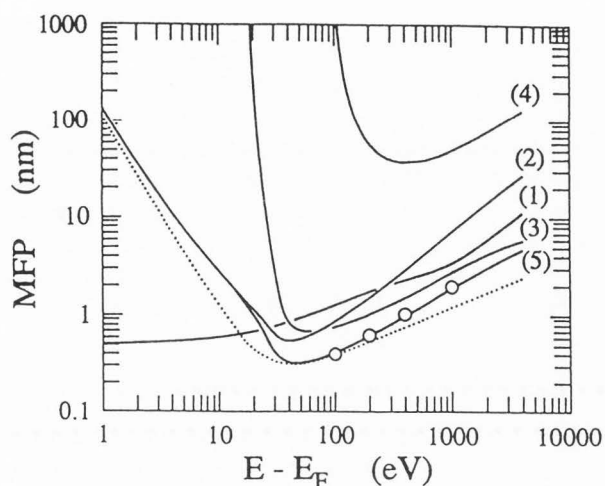
Figure 1. Calculated mean free paths (MFPs) of an electron in beryllium as a function of the energy E above the Fermi energy E_F: **(1)** elastic collision; **(2)** single conduction-electron excitation; **(3)** bulk plasmon excitation; **(4)** K-shell electron excitation; and **(5)** total inelastic collision {i.e., (2)+(3)+(4)}. The open circle and the dotted line are the total inelastic MFPs from calculation by Akkerman and Chernov [1] and those from empirical formula derived by Seah and Dench [61], respectively.

---

ions with a potential energy well above the surface work functions for multiply charged ions, it is beyond the scope of the present discussion. The PFM in fusion devices is usually bombarded by hydrogen isotopes and by heavier impurities (C, N, O and metals), which are highly ionized due to frequent collisions with plasma electrons. At very low energies, there is sufficient time for neutralization of an ion before its impact on the surface. However, if the multiply charged ion passes the crucial zone of interaction in front of the surface too fast, the time for neutralization will be so short that the ion will penetrate into the solid with a highly charged state. The resulting kinetic emission in the solid will, therefore, differ from that for originally neutral atoms with the same impact energy, and will also depend on the initial charge state.

This paper reports on our simulation of secondary electron emission due to electron bombardment and kinetic electron emission due to ion bombardment, and discusses the interaction cross-sections and energy losses of the projectiles and excited electrons used in the simulation. The energy range relevant to plasma-surface interaction is 100 eV to 10 keV. Applications to beryllium reveals some interesting similarities and differences between electron and proton bombardments. Also, the effects of initial charge state and mass of projectile on kinetic emission are discussed. Furthermore, by considering not only a flat surface but also periodic, bowl-and-ripple surfaces, surface roughness effects on the secondary electron yield, as well as the energy and angular distributions of emitted secondary electrons are elucidated.

Simulation Models and Cross-Sections for Electron- and Ion-Atom Collisions

Secondary electron emission due to electron bombardment

In the 1970's, the direct Monte Carlo simulation (MCS) based on differential cross-sections for elastic and inelastic collisions of particles in a medium was applied to electron backscattering and secondary electron emission (Shimizu *et al.* [63], and Ganachaud and Cailler [26]). Since then, the direct MCS model has been further developed by several groups [57]. Our direct MCS model of secondary electron emission involves the following inelastic collision processes of electrons in beryllium: (1) excitation of single conduction electrons; (2) excitation and decay of bulk plasmons; and (3) excitation of inner-shell (K-shell) electrons.

The excitation cross-sections of single conduction electrons and bulk plasmons ($\hbar\omega_p = 18.19$ eV) are calculated from the Lindhard dielectric function and the Drude dielectric function, respectively, according to Tung and Ritchie [72]; ω_p is the plasma frequency of the free-electron gas, and $\hbar$ is the Planck constant divided by 2π. Theoretically, multiple-electron excitation by decay of one plasmon would add to the finite width of the plasmon dispersion relation; therefore, one-electron excitation is the predominant process; the width is determined by the plasmon damping effect (e.g., interband transitions of conduction electrons) [56]. However, the plasmon, in practice, decays in the process of its propagation due to some impurities and defects of the solid and other reasons [42]. Therefore, following the treatment of Al by Cailler and Ganachaud [17], we assume an isotropic excitation of one or two electrons in the ratio 0.75:0.25 by one plasmon decay. For the K-shell electron excitation, the classical expression of the cross-section is taken from Gryzinski [27]. The calculated inelastic mean free paths of an electron in beryllium are shown in Figure 1, along with the elastic mean free path described later. The total inelastic mean free path is in good agreement with the calculation by Akkerman and Chernov [1]. The energy of liberated electrons (secondary electrons) is $\Delta E + E_F$ for excitation of single conduction electrons, and $\Delta E - E_i + E_F$ for excitation of K-shell electrons (taking into consideration the initial state of electron); here ΔE, E_i and E_F are the energy loss of primary electrons, the first ionization energy of K-shell electrons (111 eV) and the Fermi energy of

beryllium (14.08 eV), respectively. For excitation of one electron by plasmon decay, the energy of secondary electrons is distributed between $\hbar\omega_p$ and $\hbar\omega_p + E_F$, depending on the density-of-states in the conduction band, whereas, for excitation of two electrons, the energy is distributed randomly to these two electrons (taking the initial state of electron into consideration). The scattering angle of primary electrons and the emission angle of secondary electrons for excitations of single conduction electrons and K-shell electrons are calculated using the energy and momentum conservation law, whereas, for plasmon decay, an isotropic angular distribution is assumed for the emission angle of secondary electrons.

For the energy range of keV or less, when a primary electron penetrates into a solid, it undergoes a number of elastic collisions by ionic cores. At such low energies, the elastic collision cross-section should be calculated using the partial wave expansion (PWE) method with appropriate atomic potential in the solid [51]. In this study, however, the elastic collision of electrons by beryllium ionic cores is replaced by the screened Rutherford cross-section where the screening parameter {depending on the electron energy $\tau(E)$}, is fitted to the PWE cross-sections according to Fitting and Reinhardt [24]: $\tau(E) = 0.9 + \exp(-E/E_\tau)$, where E_τ is 350 eV.

Simulation of secondary electron emission is initiated by calculation of a free-flight path of a primary electron with the total mean free path suffered from these elastic and inelastic collisions and a uniform random number. Whenever a collision occurs, another random number determines the type of collision (i.e., elastic collision, excitations of a single conduction electron, bulk plasmon, or K-shell electron) in proportion to each cross-section. Other important quantities in the simulation are the scattering angle Θ in elastic collision and the energy loss ΔE in each inelastic collision event. To generate values of Θ and ΔE distributed according to the differential cross-sections of elastic and inelastic collisions, a further random number is generated. The values Θ and ΔE are selected at random according to the probability distribution function (i.e., the cumulative differential cross-section normalized by each total cross-section), except for plasmon excitation. For plasmon excitation, ΔE is chosen between $\hbar\omega_p$ and $\hbar\omega(q_c)$; q_c is the cut-off wave-vector of the bulk plasmon dispersion relation ($q_c = 1.2$ Å^{-1} in beryllium [55]).

The motion of secondary electrons generated through inelastic collisions is treated in the same manner as that of primary electrons. As a result, the secondary electrons generate new secondary electrons during their transport within the solid, which is henceforth called electron cascade. A primary electron and every secondary electron are followed in the three-dimensional space; the azimuthal angle in each collision is chosen randomly from 0 to 2π. When their energy falls below the surface potential barrier $E_F + \Phi$, or when the electrons are emitted from the surface, they are not followed any more (Φ is the work function: 4.98 eV for beryllium). Since the planar surface barrier model [40] is adopted, some of the electrons are emitted to vacuum with reduced energy in a deflected direction due to the surface potential barrier. As in the standard practice, such electrons are roughly divided into the backscattered electrons (energy greater than 50 eV) and the true secondary electrons (energy less than 50 eV).

Ion-induced kinetic electron emission

An ion impinging on the surface of a solid penetrates into the solid, losing its kinetic energy through both elastic collisions with ionic cores and inelastic collisions with atomic electrons. The basic idea of the Monte Carlo model used here is to simulate trajectories of projectile ions penetrating into the solid and of excited electrons traveling towards the surface according to given cross-sections for scattering processes. For heavy projectiles, there are also the collision processes of the recoiling solid atoms which are generated from the elastic collisions of the projectile: these excite a considerable number of electrons. For trajectory simulation of excited electrons, the direct Monte Carlo model developed for secondary electron emission under electron bombardment is used.

Trajectories of the projectile ion and the recoiling atoms are simulated by using the same algorithm as the TRIM.SP code [13]. This Monte Carlo program is based on the binary collision approximation and assumes an amorphous medium; it follows all particles (the projectile ions and recoiling atoms) in the three-dimensional space. The motion of the projectile ions and of the recoiling atoms is treated in the same way: every particle moves along a free flight path $L = N^{-1/3}$ (N is the atomic density of the target) before it encounters its next collision partner with an impact parameter P (between 0 and $\pi^{-1/2}N^{-1/3}$). At low energies, $N^{-1/3}$-Ptan($\Theta/2$) is used as L to account for the path-length reduction, where Θ is the scattering angle in the center-of-mass system [14]. The azimuthal angle and the impact parameter, which are related to the scattering angle with an approximate analytical formula including the Ziegler-Biersack-Littmark (ZBL) potential [21, 79], are determined by random numbers. The electronic energy loss in the paths between collisions is determined by the electronic stopping power calculated using the local-field correction dielectric function as described below, while the energy loss accompanying the (elastic) collision is calculated using the classical collision theory; if the elastic energy loss exceeds the displacement energy, a new recoiling atom is generated. The trajectories of a

projectile ion and all recoiling atoms are simulated until their energy falls below the surface binding energy (3.32 eV for Be), or until the ion (recoiling atom) backscatters (sputters) away from the solid surface.

The minimum energy of ions for plasmon excitation is much higher than 10 keV, and the ionization cross-section of the K-shell electron, even for proton impact, drastically decreases at energies less than 100 keV [33, 57 (p. 24-35)]. In this study, only the excitation of conduction electrons is included in the inelastic interaction with the solid. According to the Lindhard theory [47] for electron excitation, the energy-loss probability and mean free path for a projectile ion and recoiling atom are calculated using the local-field correction dielectric function from Wang and Ma [75]:

$$\epsilon(k,\omega) = 1 - [P(k,\omega)/\{1 + G(k)P(k,\omega)\}], \quad (1)$$

where $P(k,\omega)$ is Lindhard's polarizability and $G(k)$ is the correction term given by Utsumi and Ichimaru [73] in which the correlation-exchange interaction of electron gas is included. The type of collision (i.e., elastic collision or excitation of a single conduction electron) is determined in proportion to each cross-section, and only in the latter case is an electron liberated. The energy of liberated electrons is distributed between ΔE and $\Delta E + E_F$, depending on the density-of-state in the conduction band, with an upper limit of energy transferred from the ion (or recoiling atom) to an electron, according to Rösler and Brauer [57 (p. 24-35)]. The emission angle of the electrons is determined in the same manner as in the case of excitation of conduction electrons by primary electrons, whereas the scattering angle of the ion through the electron excitation is neglected. When the ion enters into a solid, it become charge-equilibrated after passing through a few top layers of the surface, in our study the distance for equilibration is assumed to be 20 Å [46], where the charge state of the ion varies linearly from the initial charge state to the effective charge of moving ions according to Wang and Ma [76].

The calculated mean free paths of various ions (H$^+$, Be$^+$, C$^+$, Ne$^+$) and a recoiling atom (Be^0) for excitation of an electron in beryllium are shown in Figure 2. The results of preliminary calculation of the proton inelastic mean free path in aluminum are connected with those of the high-energy (> 10 keV) calculation by Smidts *et al.* [65]. The probability of an electron excitation by ions is clearly much smaller than that by electrons (Fig. 1) and the probability of elastic collision by ions at such energy. Our calculated stopping power (i.e., electronic energy loss) of the ions in beryllium is in reasonable agreement with the empirical ZBL formula [79 (p. 66-108)], except at very low energies, where a
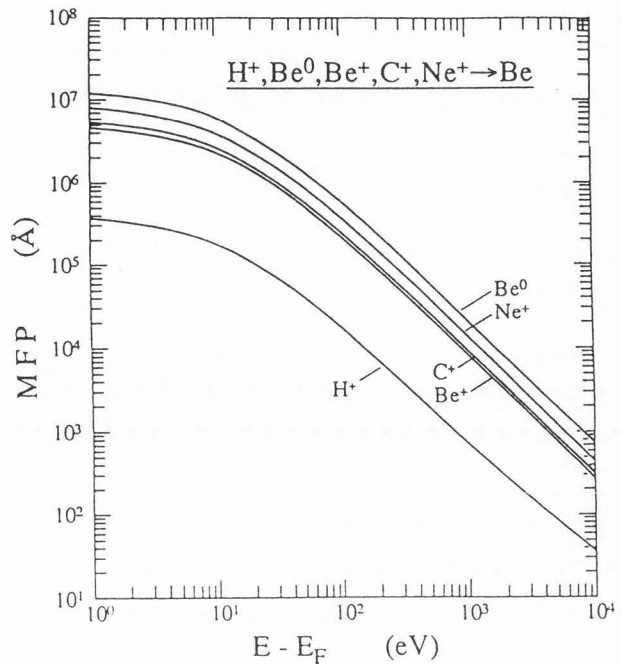

Figure 2. Calculated mean free paths (MFPs) of ions (H$^+$, Be$^+$, C$^+$ and Ne$^+$) and a neutral atom (Be^0) in beryllium as a function of the energy E above the Fermi energy E_F; single conduction-electron excitation.
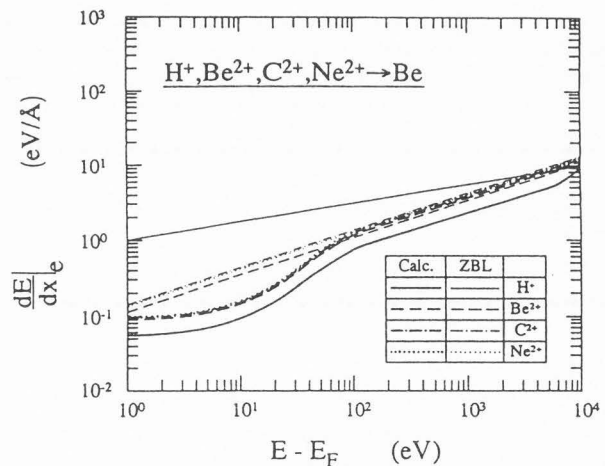

Figure 3. Calculated electronic stopping power dE/dx$|_e$ of ions (H$^+$, Be^{2+}, C^{2+} and Ne^{2+}) in beryllium as a function of the energy E above the Fermi energy E_F. The thin lines are the electronic stopping power dE/dx$|_e$ of the empirical ZBL formula derived by Ziegler *et al.* [79 (p. 66-108)], respectively.

---

deviation from the linear velocity dependence of the stopping power is found, as shown in Figure 3.

a

b
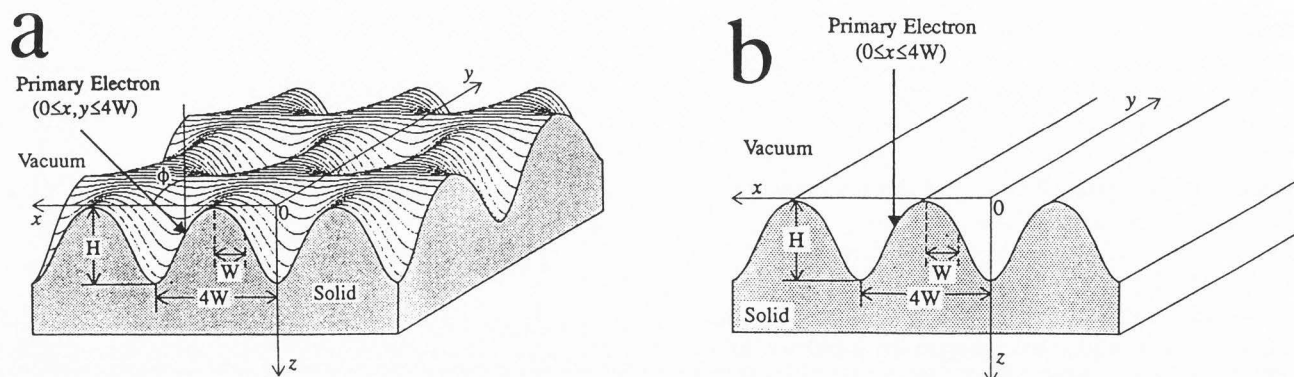
Figure 4. Models of (a) bowl structure and (b) ripple structure for surface roughness. The profile is constructed with the Gaussian distribution: (a) $z = H\exp[-\{(x-4nW)^2+(y-4nW)^2\}/W^2]$; and (b) $z = H\exp[-(x-4nW)^2/W^2]$ for $(4n-2)W \leq x,y \leq (4n+2)W$, $n = 0, \pm1, \pm2,\ldots$. The H and W are the depth and width of the depression, respectively, and 4W is the distance between two periodic structures. A primary particle is assumed to bombard at incident angle ϕ from surface normal to a macroscopic surface ($z = 0$), and the bombardment point is uniformly chosen over the range of x and y ($0 \leq x,y \leq 4W$).


Models for surface roughness

Elementary models of bowl-and-ripple structures schematizing rough surface are designed as shown in Figures 4a and 4b, respectively. The profile of the surface is constructed with the Gaussian distribution. By high-fluence plasma particle (or ion) bombardment, solid surfaces are strongly modified, and as a result, large roughnesses, with depression of the width $W \geq 100$ nm and the depth $H = 100$ nm to 10 μm, are observed [5]. The values of H and W are chosen in this study to include not only large roughnesses but also atomic scale roughnesses (≤ 10 nm), which are comparable to the maximum range R of primary electrons (e.g., $R \approx 11.8$ nm for 300 eV electrons in beryllium [23]). The bombardment point is randomly chosen over the ranges of x ($0 \leq x \leq 4W$) and y ($0 \leq y \leq 4W$). Reflection and deflection of primary and secondary electrons at the rough-textured surfaces are taken into account by applying the planar surface barrier model to the microscopic boundary of the surface. Furthermore, due to topographic features of the surface, re-entrance of electrons once emitted from the surface into the other part of the solid and then re-emission from the other surface are taken into account. The incident angle ϕ of the projectile and the emission angle of secondary electrons finally escaping into vacuum are measured from the normal of the macroscopic surface (z-axis); the incident angle is changed in the plane including incident particle (the x-z plane).

Results and Discussion

### Comparison of electron emission between electron and proton bombardments

Our calculated values of the true secondary electron
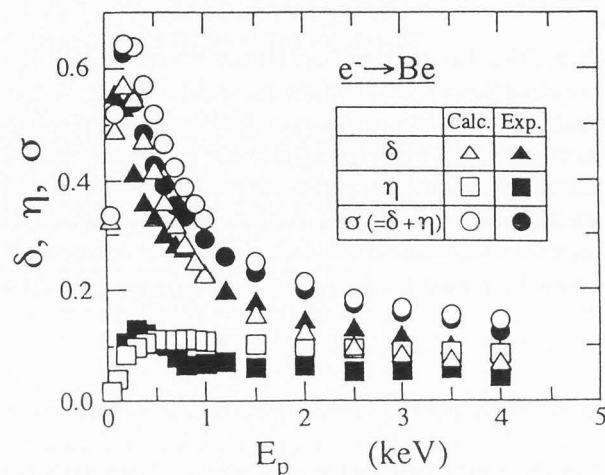
Figure 5. Secondary electron yield δ, backscattering coefficient η, and the total electron yield σ of beryllium for electron bombardment, as a function of the impact energy E_p ($\phi = 0°$). The open symbols data are from our calculation, the solid symbols data are from an experiment by Bronshtein and Dolinin [15].

----

yield δ, the backscattering coefficient η, and the total electron yield σ of beryllium by electron bombardment at normal incidence are shown in Figure 5, together with experimental results of Bronshtein and Dolinin [15]. A hump is observed at around 200 eV in the experimental data of the backscattering coefficient due to an influence of electrons elastically backscattered [59]. An oscillatory feature of the "exact" elastic PWE cross-section causes the hump [34], whereas, the screened Rutherford cross-section used in our calculation smoothed it out due to a high energy Born approximation. For aluminum and other materials, the hump may disappear in many backscattering electrons ($\eta > 0.2$) suffered from
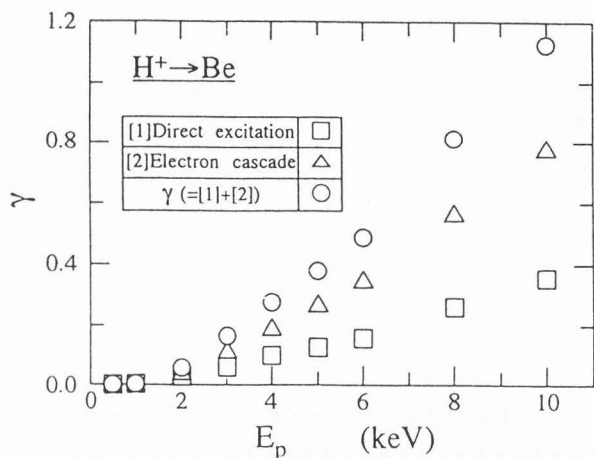
Figure 6. Kinetic electron yield γ of beryllium for proton bombardment, as a function of the impact energy E_p ($\phi = 0°$). The squares and triangles represent emission of electrons excited by a projectile proton and an electron cascade, respectively, and the circles are the sum of them.

----

inelastic collisions. The calculated total electron yield agrees well with experiment at every impact energies. At high impact energies, however, the calculated true secondary electron yield (backscattering coefficient) is smaller (larger) than experimental values. Suleman and Pattinson [68] also observed the maximum (total) electron yield of 0.68 at the impact energy of 200 eV, and Darlington [18] observed the backscattering coefficient of 0.05 at 9.3 keV; the former is consistent with our calculation, but the latter is not. The calculated electron yield is sensitive to the cross-sections for elastic and inelastic collisions of electrons in a solid. For the simulation of the secondary electron emission from aluminum, Dubus *et al.* [20] emphasized the importance of the description of elastic collisions, of the choice of the dielectric function, and of the role of ionizing collisions. However, we should qualify discussion on the difference between the calculated and experimental values, since, we assume ideal surface conditions. The roughness of solid surfaces will be a possible reason for the discrepancy, although the secondary electron emission is sensitive to surface contamination, which may lead to the change in the surface potential barrier (i.e., work function) [68]. As expected, the surface roughness causes a dispersion of incident angle of primary electrons. As demonstrated later, usually observed roughnesses with the aspect ratio H/W < 1 result in larger secondary electron yield in comparison with that for an "ideally" flat surface, because of substantial increase in the electron yield with an inclined incidence [70]. However, specularly backscattered (reflected) electrons from an inclined surface re-enter into the neighboring part of the

surface topography; this effect decreases the backscattering coefficient.

There is a clear difference, to be theoretically expected, in the energy dependence of the electron yield between electron and proton bombardments in the keV range, because of a large difference between electron and proton masses. At a given impact energy, the initial velocity of a primary electron is about two order of magnitude larger than that of a proton. This causes a large difference between the cross-sections (or mean free paths) for an electron excitation by electrons and by protons (e.g., see, Figs. 1 and 2). In general, therefore, the secondary electron yield has a maximum for primary electron energies below 1 keV, whereas the corresponding maximum is at about 100 keV for proton bombardment [70] and higher for heavy-ion bombardment. As a result, in the keV energy range, the secondary electron yield for electron bombardment becomes small as the impact energy is increased, whereas an opposite trend is found for proton bombardment as shown in Figure 6. Hasselkamp *et al.* [30] obtained the electron yield of beryllium by impact of 100 keV protons, and gave the ratio of the yield γ to the electronic stopping power $dE/dx|_e$ as 0.078 ($\pm$ 0.003). Using the ratio together with our calculated stopping power (Fig. 3) or the ZBL stopping power [79 p. (66-108)], one can estimate the electron yield at 10 keV as approximately 0.7-0.8, which is smaller than our electron yield. This may cause an excess cascade multiplication of the excited electrons in our simulation, although, at such low energies (< 10 keV), the ratio $\gamma/(dE/dx|_e)$ depends upon the impact energy [2, 37].
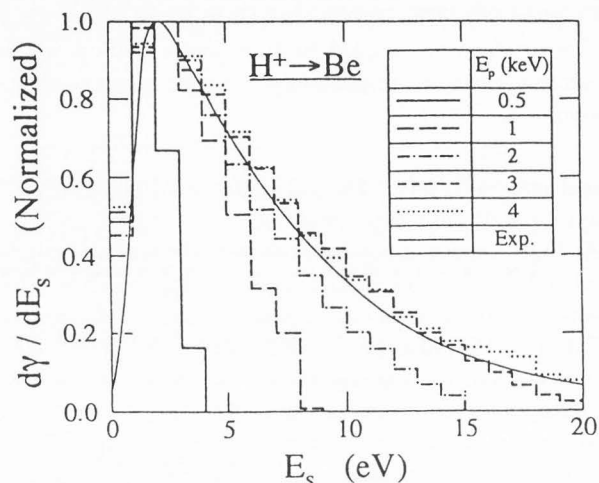
In spite of this difference between the energy dependences of the electron yield by electron and proton bombardments, the shape of the calculated energy distributions of electrons emitted in vacuum are similar (Figs. 7 and 8), as reported recently [28, 29, 31 (p. 58-65)]. This is because the majority of electrons emitted from the surface are produced through the cascade of electrons excited by projectile particles within beryllium (see Fig. 6). The energy distributions have a peak at an energy of less than 5 eV. Its location depends slightly on the energy of the projectile, whereas the shape of the distribution depends on the energy differently for electron and proton bombardments. With increasing energy for electron bombardment, the high-energy component of the distribution decreases; for proton bombardment the opposite trend is calculated, as obtained experimentally [28, 29, 31 (p. 58-65)]. This difference between electron and proton bombardments is understood also from the cross-section (mean free path) for an electron excitation by electrons and protons (Figs. 1 and 2). For electron bombardment, as the impact energy increases, most secondary electrons are produced in deeper regions

Table 1. Excitation depth distributions of electrons emitted from beryllium for 1-4 keV electron and proton bombardments.

Ep (keV)		0-20	20-40	Excitation depth (Å) 40-60	60-80	80-100	100-∞
1	e^-	78.11%	17.27%	3.40%	0.79%	0.23%	0.20%
	H^+	80.68%	16.34%	2.44%	0.49%	0.02%	0.03%
2	e^-	77.83%	15.33%	3.40%	1.16%	0.57%	1.71%
	H^+	80.99%	15.96%	2.52%	0.42%	0.11%	-
3	e^-	75.48%	15.12%	3.31%	1.33%	0.67%	4.09%
	H^+	81.70%	15.12%	2.60%	0.48%	0.09%	0.01%
4	e^-	74.14%	14.83%	3.14%	1.26%	0.77%	5.86%
	H^+	81.75%	15.12%	2.56%	0.50%	0.05%	0.02%
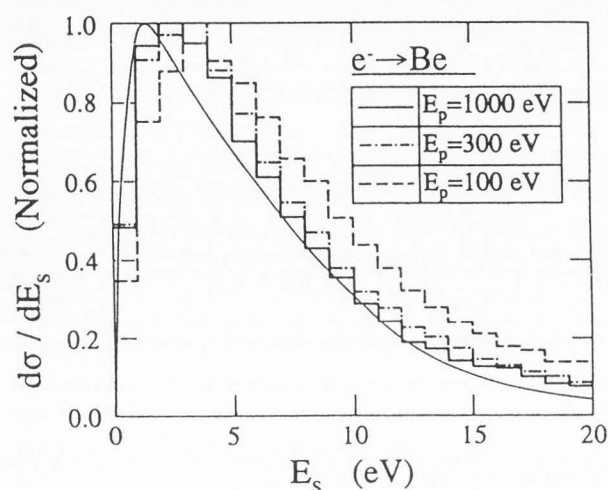
Figure 7. Energy distributions of secondary electrons emitted from beryllium for electron bombardment ($\phi = 0°$). The thin solid curve is an experimental distribution for $E_p = 960$ eV, obtained by Koshikawa *et al.* [41].

Figure 8. Energy distributions of electrons emitted from beryllium for proton bombardment ($\phi = 0°$). The thin solid curve is an experimental distribution for $E_p = 500$ keV, obtained by Hasselkamp *et al.* [29].

of the solid, where the energy of a primary electron is reduced to several tens of eV, and the excited electrons lose more energy due to many inelastic collisions in their transport to the surface. For proton bombardment, most of secondary electrons are excited in shallower regions of the solid, where an ion is more energetic and excited electrons lose less energy. The calculated distributions roughly agree with the observed ones [29, 41]; for electron bombardment, however, the peak position shifts ≈ 1 eV towards the high-energy side, and the shape of the distribution is slightly broader than the observed distributions [41]. For resolving this disagreement, detailed discussions on our models (e.g., energy and angular distribution of each electron excitation process) should be done [17, 35]. For example, an increase in the excitation probability of two or more electrons by a plasmon

decay produces more low-energy electrons to be emitted, because the plasmon energy is distributed among more electrons. This lowering of the energy distribution results in an increase in the secondary electron yield at the same time. Furthermore, when surface roughness is considered in our simulation, the distribution is expected to shift towards the low-energy side, as described later.

It is also found that secondary electrons emitted from the surface originate mainly within a depth of less than 40 Å (Table 1). This is consistent with experimental data of low-energy electron escape depth for metals by Seiler [62] and theoretical calculations by Ono and Kanaya [53] (the most probable escape depth ≈ 31 Å). Furthermore, secondary electrons emitted from larger depths increase as the impact energy is increased since the mean energy of secondary electrons becomes large
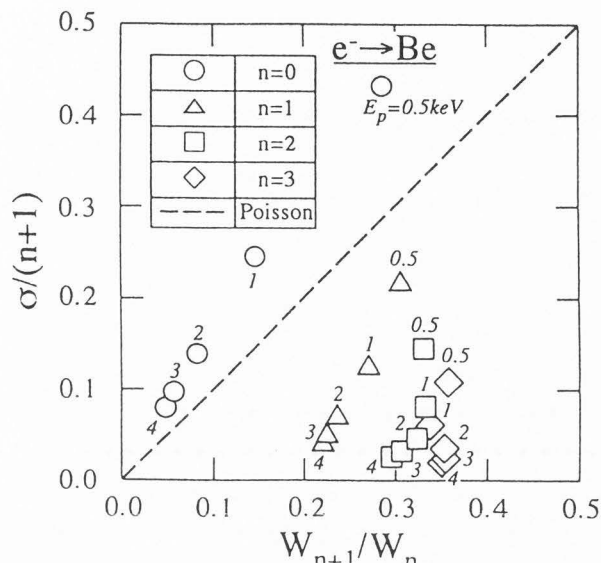
Figure 9. Relation between $\sigma/(n+1)$ and W_{n+1}/W_n for impact of 0.5-4 keV electrons on beryllium, showing the deviation of electron emission statistics from the Poisson distribution (shown by the broken straight line).
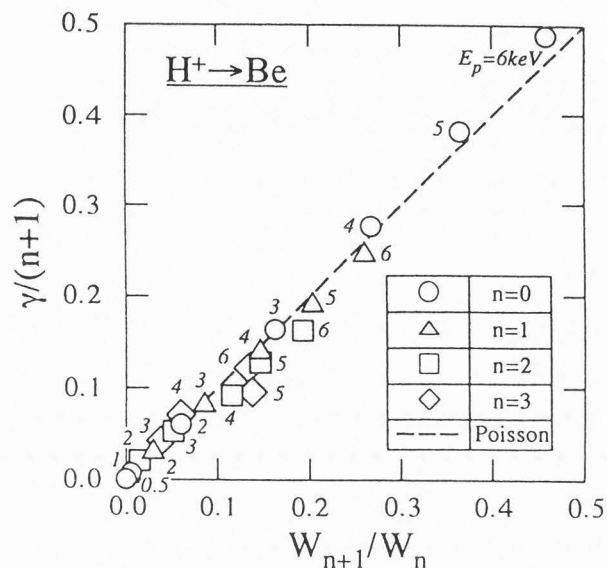

Figure 10. Relation between $\gamma/(n+1)$ and W_{n+1}/W_n for impact of 0.5-6 keV protons on beryllium, showing the deviation of electron emission statistics from the Poisson distribution (shown by the broken straight line).

---

with increasing projectile energy. Electron excitations by protons occur near the surface before the protons lose much of their energy since the cross-section (mean free path) of the electron excitation decreases (increases) with decreasing energy. Also, the energy of electrons excited by keV protons is below 100 eV, which is much smaller than that by primary electrons. It is difficult for the low-energy electrons excited in a deep region to escape from the surface due to strong elastic and inelastic interactions in beryllium. As a result, kinetic electron emission by proton bombardment is shallower than secondary electron emission by electron bombardment.

Since all electron emission processes are subject to statistical fluctuations, the secondary electron yield is the mean of a statistical distribution over the individual probabilities W_n for emission of n = 0, 1, 2, 3, ... electrons per impinging projectile particle. In many experiments [4, 7, 11, 12, 19, 39, 43, 44, 77], statistics of ion-induced kinetic electron emission was investigated and considerable deviations from the Poisson distribution $P_n(\gamma)$ with the mean value γ,

$$P_n(\gamma) = (\gamma^n / n!) \exp(-\gamma), \qquad (2)$$

were observed. As already shown [52, 77], a critical comparison of the electron emission statistics with the Poisson distribution can be made by plotting ratios of relative probabilities W_{n+1}/W_n versus the corresponding expressions of the related Poisson distribution:

$$P_{n+1} / P_n = \{\gamma / (n+1)\}. \qquad (3)$$

In Figures 9 and 10, we show such relations obtained from the present simulation for beryllium bombarded by electrons and protons, respectively. The deviations of the electron emission statistics from the Poisson distribution are similar to those previously described for gold bombarded by protons [52]. The ratios W_{n+1}/W_n for $n \geq 1$ are greater than the Poisson values, whereas the ratios for n = 0 are smaller. These deviations result from both a larger W_0 and larger W_ns for higher n emission ($n \geq 2$).

The backscattering of projectile particles causes two effects on the particle-induced electron emission: one is an additional excitation of electrons near the surface by the projectile on its way out, and the other is backscattering immediately after incidence without exciting electrons. The former produces the high n emission and the latter produces the large W_0. For beryllium, the backscattering coefficient is very small for electrons and protons; therefore, the deviation from the Poisson distribution due to the backscattering effects is small.

In general, the electron multiplication due to the cascade process produces the high n emission in the electron emission statistics; the probability W_n ($n \geq 2$) increases. However, excess multiplication decreases the kinetic energy of each electron so that fewer electrons can be emitted from the surface through the surface potential barrier; then, the probability W_0 increases. Furthermore, at high impact energies, electrons excited by the electron cascade have difficulty in escaping from the surface due to the deep generation depth leading to

339

strong interactions with the ionic cores and conduction electrons. Therefore, with increasing impact energy, the deviation of the probability W_0 (i.e., W_1/W_0) from the Poisson distribution is enhanced. Electron emission statistics for electron bombardment largely deviate from the Poisson distribution, in comparison with those for proton bombardment. The energy transferred from a projectile to a secondary electron for electron bombardment is much larger than that for proton bombardment. This results in stronger multiplication of secondary electrons in the electron cascade process, as a result, the larger W_n ($n \geq 2$) and larger W_0 are produced.

Heavy-ion-induced kinetic electron emission

Potential emission (PE) occurs for positive-ion bombardment even at a very low impact energy if the potential energy of the ion exceeds twice the work function of the metal surface. Kinetic emission (KE) occurs inside the solid both for ions and neutral atoms if they give metal electrons sufficient kinetic energy to overcome the surface potential barrier. As a result, KE is subject to an impact energy (velocity) threshold. To a first approximation, the KE threshold energy is conventionally calculated from the condition that the maximum energy transfer from a projectile ion in a head-on collision with a nearly free conduction electron is equal to the surface work function: $E_{th} = (1/2)m_p v_{th}^2$ and $v_{th} = (1/2)v_F\{(1 + \Phi/E_F)^{1/2} - 1\}$, where m_p and v_F is the projectile mass and the Fermi velocity, respectively. Thus, for a beryllium surface, the KE threshold energy is about 172 eV/u (where "u" = unified mass unit). As shown in Figure 11, our calculated KE yield decreases with decreasing impact energy and with increasing mass of the projectile ion, due to insufficient excitation of electrons (Fig. 2) and due to small energy transferred to the electrons, respectively, and it vanishes at the conventional KE threshold: 172 eV for H^+, 2058 eV for C^+, and 3429 eV for Ne^+; the heavier the ion is, the higher is the threshold energy. Elastic collisions with ionic cores will cause the projectile ion to lose some of its kinetic energy and therefore to excite less electrons, whereas they produce sufficiently energetic recoiling atoms that can produce electron excitation. Therefore, as described in many publications [9, 31 (p. 30), 33, 60], an additional contribution of recoiling atoms on KE is expected to arise for heavy-ions (C^+ and Ne^+) in a low-atomic-number solid as beryllium, due to a smaller KE threshold energy: 1545 eV for excitation of electrons by recoiling Be atom. However, within our conventional model of conduction electron excitation by recoil atoms, the contribution to the total KE yield is very small, as was the case for the light ions. This can be explained, within our model calculations, to result from few large-angle scattering of the projectile ion, produc-
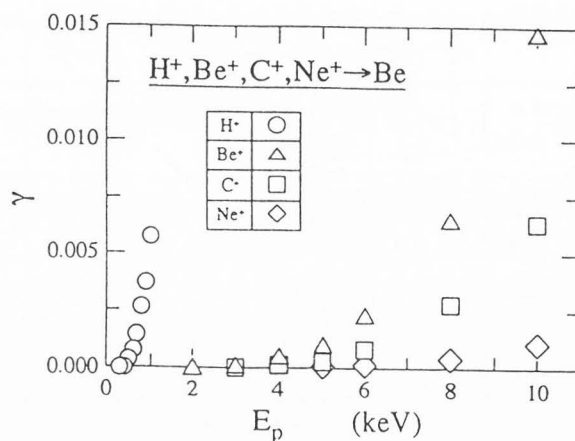

Figure 11. Kinetic electron yield γ of beryllium for ion (H^+, Be^+, C^+ and Ne^+) bombardments, as a function of the impact energy E_p ($\phi = 0°$).

----

ing recoiling Be atoms with the energies of more than the KE threshold (1545 eV), near the surface (≤ 20 Å). Other mechanisms, e.g., electron promotion, as discussed below, may also be important for electron excitation by recoil atoms, as well as the projectile ion, in the solid.

Recent investigations for heavy-ion impact on clean polycrystalline gold have revealed a considerably smaller KE threshold energy (10 eV/u) than the conventional value [3, 45]. For keV heavy-ions, the inner-shell electron excitation by electron promotion in projectile-atom collisions, proposed by Ploch [54], may be the dominant process of KE [6, 8, 33]. If the collision between the ion and a solid atom proceeds closely, a temporary molecule can be formed. One or more inner-shell electrons may be excited into the conduction band and emitted from the atoms during the collision. Since the energy of electrons liberated by the electron promotion mechanism stems from excited solid and/or projectile atoms, just as inelastic processes involving atoms in the gas phase [2], it will be considerably higher than that transferred directly from a head-on collision of the projectile with an electron. In fact, the measurements by Baragiola et al. [10] show that the energy distribution of emitted electrons extends up to a surprisingly large fraction of the center-of-mass energy, which results from nearly head-on collisions between the projectile and a solid atom. By choosing the maximum energy E_m of excited conduction electrons to $4m_p m_t/(m_p + m_t)^2 E$, the ion will be found to produce KE at much lower impact energies than the conventional threshold [36]; here m_p and m_t are the masses of projectile ions and target solid atoms, respectively, and E is the instantaneous projectile energy in the solid. This convenient approximation of the electron promotion with the large E_m ($\approx 0.56E$) for Ar^{q+}
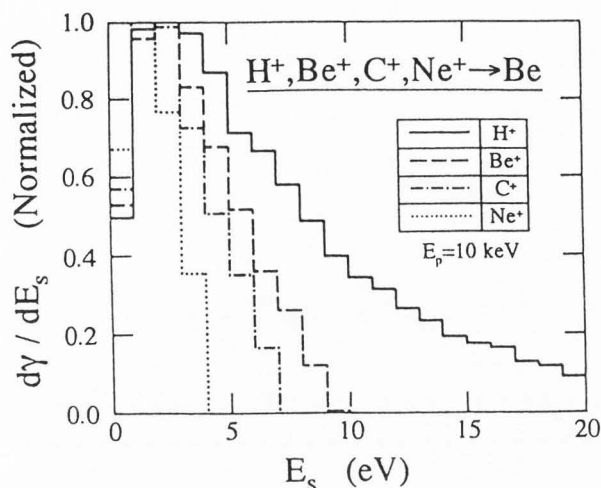
Figure 12. Energy distributions of electrons emitted from beryllium by ion (H^+, Be^+, C^+ and Ne^+) bombardments at $E_p = 10$ keV ($\phi = 0°$).

Figure 13. Kinetic electron yield γ of beryllium for C^{q+} (q = 0, 1, 2 and 4) bombardment, as a function of the impact energy E_p ($\phi = 0°$).

(q = 1, 2) impact on Au gives a much lower threshold than the conventional KE threshold of 4.7 keV, which is consistent with recent measurements (10 eV/u) [45].

The energy distribution of electrons emitted into vacuum generally presents a high peak at several eV followed by a monotonically decreasing tail. The full width at half maximum (FWHM) of this peak slowly increases with the ion energy. Oda *et al.* [50] measured the energy distribution of electrons emitted from clean Ta by keV noble-gas atoms. Since the projectiles are neutral and mainly in their ground state, the distributions correspond to KE. At 5 keV, the peak of the distributions, around 2-3 eV, occurs at progressively lower energies as the projectile becomes heavier, from He to Kr. There is also a longer high-energy tail that is more pronounced for the lighter projectile. As an example, in Figure 12, we present the distributions calculated with irradiation of beryllium by H^+, Be^+, C^+ and Ne^+ ions. The variation of the calculated energy distribution agrees with the experiment. This may be understood from decrease in the maximum energy of primary electrons excited by heavier projectiles: $E_m \approx 2m_e\{v_p + (v_F/2)\}^2$ where m_e and v_p are the electron mass and the projectile velocity, respectively [57 (p. 24-35)]. At impact energy $E_p = 10$ keV, the maximum energy E_m is 71 eV for H^+, 28 eV for Be^+, 26 eV for C^+, and 23 eV for Ne^+. This results from the larger difference of the masses between the projectile ion and the excited electron.

Once the ions (or neutrals) enter into a solid, they become charge-equilibrated after passing through a few top layers (< several tens Å) of the surface. If Coulomb interaction prevails, as in the high-energy range (< 1 MeV), the KE yield should be proportional to the
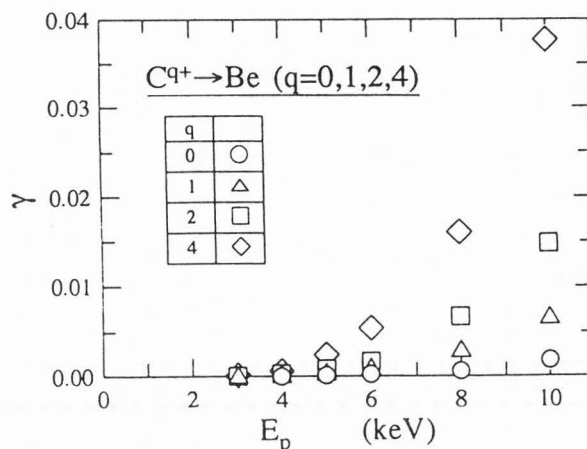
square of the charge state of the projectile for a given target material and at the same projectile velocity. For impact energies below 100 keV, however, no effect of the ion was observed for KE [31 (p. 71-74)]. This is understandable if all ions are neutralized in front of the surface by multiple resonance neutralization. If the ion passes the crucial zone of interaction in front of the surface too fast, the neutralization will not be complete, especially for highly charged ions, so that the ion is partially neutralized and penetrates into the solid with a certain charged state. Recently, Vana *et al.* [74] allowed the separation of KE contribution from PE by fitting velocity-dependence of total electron yield to an empirical expression near the KE threshold region. Their results showed that the KE contribution also depends on the initial charge state q, as well as the PE contribution. In our treatment of KE from metals under slow ion impact, the nearly-free-electron model describes the conduction electron in a first-order approximation. The stopping power calculated using the model is generally in good agreement with the empirical formulae even at the energies of 100 eV (Fig. 3), and in general, it also shows a clear q-dependence as expected (not shown here). As shown in Figure 13, as the initial charge state, or the impact energy, is increased, our calculated KE yield becomes large due to the enhanced probability of electron excitation by the projectile ion. This q-dependence of the KE yield shows a trend opposite to that observed by Vana *et al.* [74], who explained their results by the electron promotion mechanism described above.

Further, information on the heavy-ion-induced electron emission at low impact energies near the KE threshold, where the differentiation between PE and KE is difficult, can be obtained using the electron emission

341
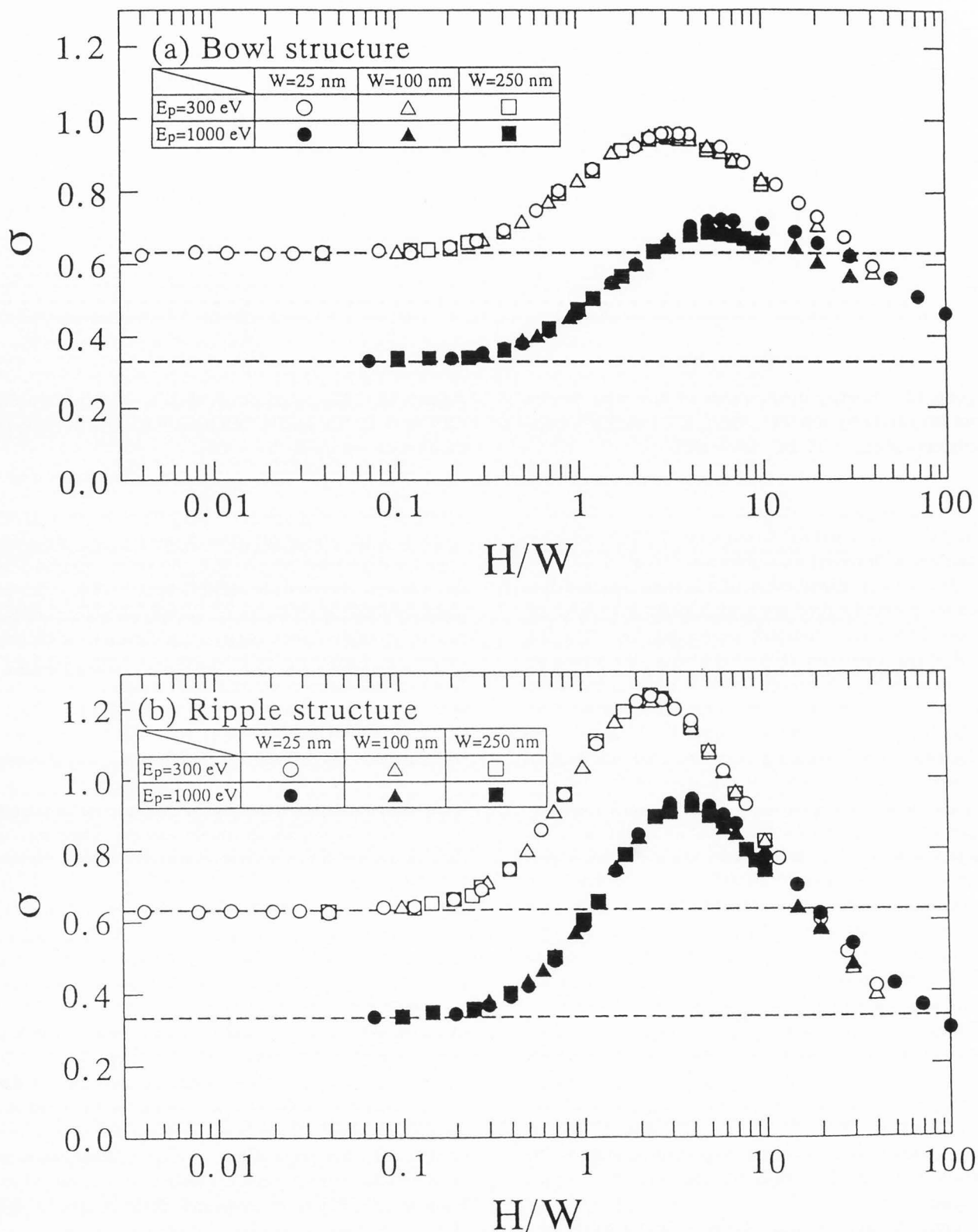
Figure 14. Variations of the secondary electron yield σ at normal incidence ($\phi = 0°$) with the roughness parameter H/W for surface roughness of bowl structure (a) and ripple structure (b). The data points are calculated by changing the depth H under the condition that the width W is constant.

statistics (ES). The KE process is based on a random series of elastic and inelastic collisions of the projectile particle, recoiling atoms, and excited electrons in the solid. Therefore, for the calculated ES, there is a large spread (wider than the Poisson distribution) in the number of emitted electrons, and the probability for emission of each number of electrons decreases with decreasing impact energy. On the other hand, the PE process can eject electrons, the number of which is dependent on the charge state of ions approaching a solid surface (or the potential energy); this number never vanishes, even at very low energy ($<$ 100 eV), as we demonstrated recently [36]. The energy and angular distributions of low-energy electrons ($<$ 20 eV) emitted from metal surface under multi-charged heavy-ion bombardment (as well as under electron and proton bombardments) for a given ion species and impact energy are the result of an electron cascade process. The gross features of the calculated distributions are, therefore, independent of the initial charge state, so long as the electron cascade multiplication is sufficiently developed in the solid.

Surface roughness effect on secondary electron emission

For electron bombardment, the total secondary electron yield σ is shown in Figures 14a and 14b for bowl- and ripple structured surfaces, respectively, as a function of the aspect ratio H/W of the roughness; these are calculated by changing H and keeping W constant. The yield σ includes backscattering electrons ($\geq$ 50 eV). For a flat surface, the yield δ of true secondary electrons ($\leq$ 50 eV) is calculated as 0.54 at primary electron energy E_p = 300 eV (σ = 0.63), whereas the backscattering coefficient η is 0.092. With increasing H/W, σ becomes greater than that for the flat surface, whereas for large H/W, σ is smaller. As long as primary electrons are normally incident on the macroscopic surface, the following effects of surface roughness on the physical processes in the secondary electron emission are considered: (1) low-energy electrons, which cannot escape from a flat surface due to energy loss during their transport to the surface and deflection of the electron trajectory by the surface potential barrier, can escape from an inclined plane of the rough surface; we henceforth call this "effect of an inclined surface"; and (2) the secondary electrons emitted from the surface with large emission angles re-enter into an adjacent part of the surface topography; this effect is henceforth called "effect of re-entrance". For small H/W, the "effect of an inclined surface" causes an increase in σ. With increasing H/W, a part of the secondary electrons emitted near the bottom of the rough surface begins to re-enter into the adjacent part of the surface; this leads to a maximum variation of σ with H/W. For large H/W, this effect of re-entrance

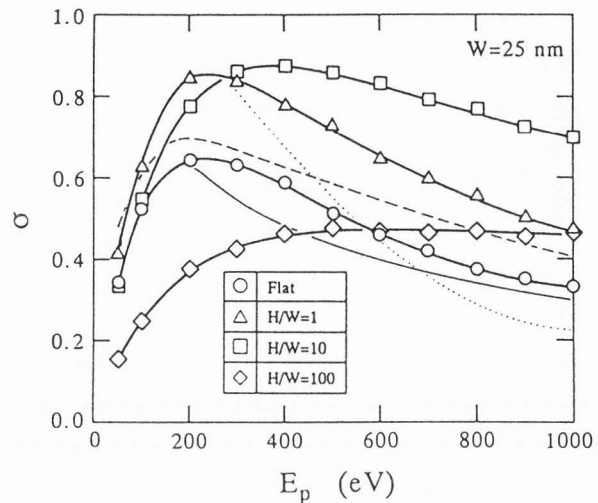**Figure 15.** Impact energy (E_p) dependence of the secondary electron yield σ at normal incidence (ϕ = 0°) calculated for a flat surface and for bowl-structured surfaces with different H/Ws. Experimental data: solid curves: Bronshtein and Dolinin [15]; dotted curve: Forman [25]; dashed curve: Suleman and Pattinson [68].

---

is dominant so that σ becomes smaller than that for the flat surface.

For bombardment of low-energy electrons, since the spatial distribution of trajectories of the electrons (e.g., the electron range R) in the solid is much narrower than H and W (R $\approx$ 11.8 nm in Be at E_p = 300 eV [23]), the two effects of surface roughness are related only to the type of topography (e.g., ripple, bowl, fractal, etc.), being independent of H and W. For ripple-structured surfaces, secondary electrons emitted perpendicularly to the rippled direction (x-direction) never re-enter the surface, whereas for bowl-structured surface, a part of the microscopic surface is partially flat. The former causes a higher peak in σ as H/W varies for the ripple structure, and the latter causes a lower peak and a slower change in the σ-variation for the bowl structure. For bombardment of high-energy electrons, since the trajectory distribution becomes large {it can be comparable or larger than W (R $\approx$ 56.2 nm at E_p = 1 keV [23])}, the two effects of surface roughness cannot be clearly distinguished from each other; furthermore, re-entered electrons may be re-emitted from opposite side of the surface; as a result, σ largely depends on H and W.

Experimental data for σ are relatively few as compared to those for heavy-particle backscattering and sputtering; the data show large scatters among experiments; e.g., at E_p = 300 eV, 0.54 (Bronshtein and Dolinin [15]), 0.83 (Forman [25]) and 0.67 (Suleman and Pattinson [68]). Since the change in calculated σ due to change in H/W is larger than the scatter of the σ data, the surface roughness of target materials may be
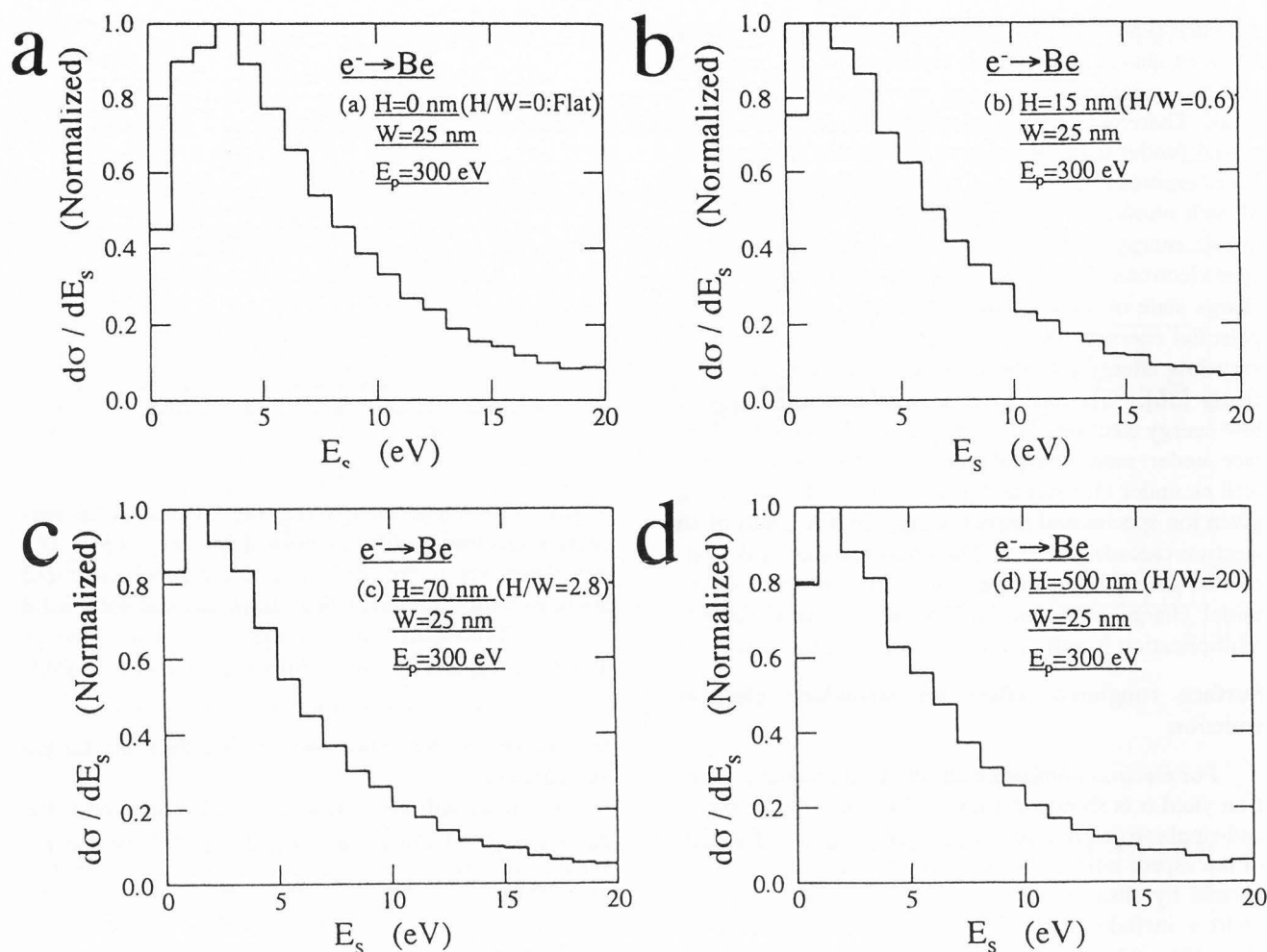
Figure 16. Energy distributions of secondary electrons emitted from flat and bowl-structured beryllium surfaces with different depths H and constant width W = 25 nm (E_p = 300 eV, ϕ = 0°): (a) H = 0 nm (H/W = 0: flat); (b) H = 15 nm (H/W = 0.6); (c) H = 70 nm (H/W = 2.8); and (d) H = 500 nm (H/W = 20).


one of the possible reasons for the large scatter in the experimental data. However, since the majority of the secondary electrons have energies below 20 eV, the calculated σ is strongly affected by the surface potential barrier, the magnitude of which is taken as 19.06 eV in this study. As a result, a more important reason for the large scatter in the experimental data may be surface contamination, which leads to a change in the surface potential barrier (i.e., the work function). For example, Suleman and Pattinson [68] observed that the maximum yield σ is 0.68 for a clean Be surface, and changes to 4.16 upon oxidation.

Figure 15 shows the energy dependence of the calculated σ as a function of H/W for bowl-structured surfaces, along with that for a flat surface. For small H/W, due to the dominant effect of the inclined surface, σ is larger than that for the flat surface (in all the energies E_p calculated), whereas, for large H/W, σ is

smaller (larger) at low (high) E_p because of fast (slow) decrease in σ with increasing H/W. As a result, the decrease in σ with increasing E_p ($\geq$ 200 eV) is suppressed because of large roughness, and σ is approximately independent of E_p (300-1000 eV) for the largest H/W (= 100).

The increase in σ due to the effect of the inclined surface should be accompanied by an increase of the low-energy component in the energy distribution, since low-energy electrons that cannot escape from the flat surface due to inelastic energy loss during their transport to the surface, can escape from an inclined plane of the rough surface. On the other hand, the effect of re-entrance decreases secondary electrons with large emission angles. In Figures 16 and 17, the energy and angular distributions of emitted electrons are shown for bowl-structured surfaces of H/W = 0 (flat), 0.6, 2.8 and 20 at E_p = 300 eV, ϕ = 0° and W = 25 nm; for which σ
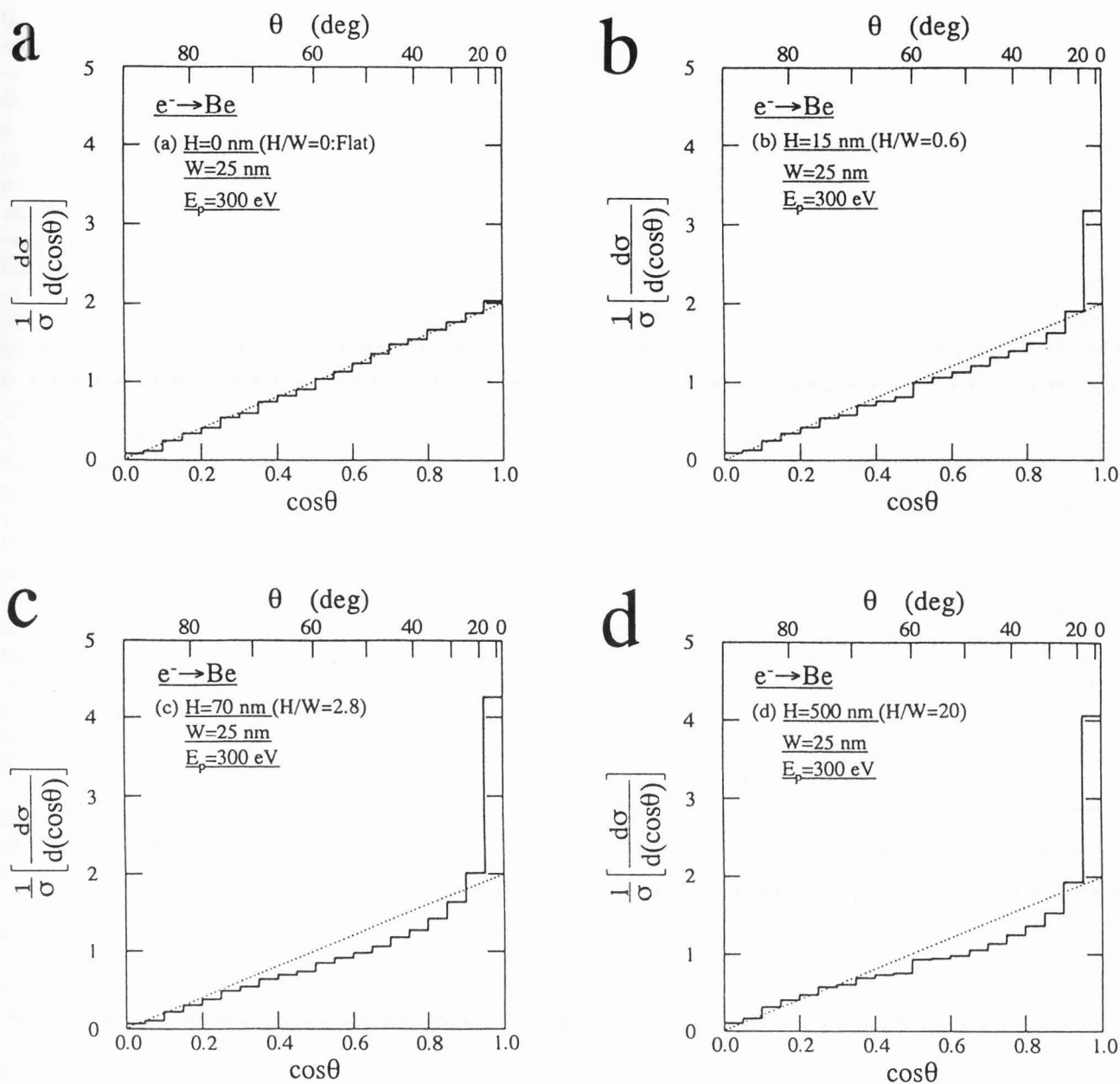
Figure 17. Angular distributions of secondary electrons emitted from flat and bowl-structured beryllium surfaces with different depths H and constant width W = 25 nm (E_p = 300 eV, ϕ = 0°): (a) H = 0 nm (H/W = 0: flat); (b) H = 15 nm (H/W = 0.6); (c) H = 70 nm (H/W = 2.8); and (d) H = 500 nm (H/W = 20). The dotted straight lines represent the cosine distribution: the number of electrons emitted in a unit solid angle is proportional to $\cos\theta$ (θ: the emission angle measured from the surface normal).

----

is 0.63, 0.75, 0.97 (maximum) and 0.73, respectively. The effect of the inclined surface is dominant in the case of Figure 16b and the effect of re-entrance is clearly observed in the case of Figure 16d, although, in these two figures, the energy distributions as well as the values of σ are approximately the same. However, backscattering of primary electrons, which produces a small contribu-

tion to total electrons emitted, slightly increases with increasing H/W, and tend to decrease with further increasing H/W due to the dominant effect of re-entrance; the backscattering coefficient η is 0.092 (flat), 0.094 (H/W = 0.6), 0.090 (H/W = 2.8) and 0.061 (H/W = 20). The angular distribution of electrons emitted from the flat surface agrees well with a cosine distribution
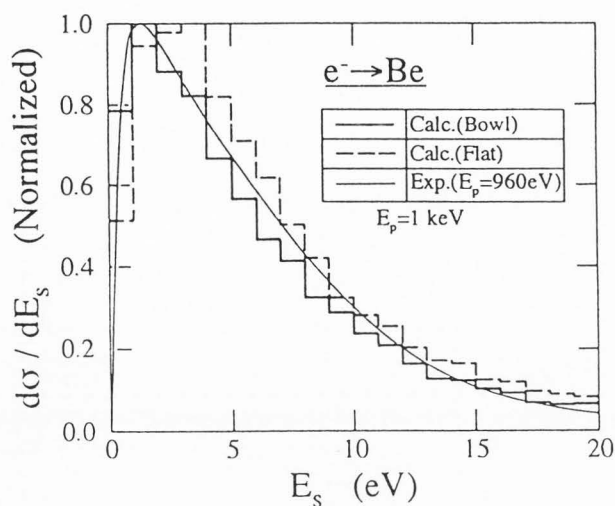
Figure 18. Comparison of the energy distribution of electrons emitted from a bowl-structured surface (E_p = 1 keV, $\phi = 0°$, H = 10 nm, W = 25 nm: H/W = 0.4) with the distribution obtained by Koshikawa *et al.* [41]. The solid and dashed lines correspond to the energy distributions emitted from the bowl and a flat (H/W = 0) surface, respectively, whereas the thin line corresponds to the experimental one.

(shown by the dotted straight line in Fig. 17): the number of electrons emitted in a unit solid angle is proportional to $\cos\theta$ (θ is the emission angle measured from the surface normal). The physical origin of the cosine distribution is an isotropic spatial development of the electron collision processes in a solid. On the other hand, secondary electrons emitted from the bowl-structured surface (in particular, from the bottom of the surface) with large emission angles, re-enter the adjacent surface. This effect of re-entrance leads to angular distribution of over-cosine type (i.e., enhanced emission in the normal direction). By introducing surface topography, the peak position of the energy distribution of secondary electrons varies from 2-3 eV to 1-2 eV, and the distribution becomes narrow. These changes result in better agreement with the observed distribution [41] (Fig. 18), although, for large H/W, the distribution is narrower than the observed one. Figure 19 shows the doubly differential electron yields $d^2\sigma/dE_s d\theta$ calculated with respect to the energy E_s and angle θ of electrons emitted from flat and bowl-structured surfaces for normal incidence.

The incident angle ϕ has a strong influence on secondary electron emission. By changing the incidence from normal to oblique angles, the path length of the projectile within an electron escape depth is prolonged, and thereby, the deposition of energy with excitation of

secondary electrons (also the secondary electron yield) increases. A simple geometric model [67], which assumes constant excitation of electrons along the projectile trajectory in the electron escape depth and disregards the elastic scattering of the projectile, leads us to a simple relation, $\sigma(\phi)/\sigma(0) = (\cos\phi)^{-1}$ (i.e., inverse cosine law); here $\sigma(\phi)$ and $\sigma(0)$ are the secondary electron yields at an incident angle ϕ and at normal incidence, respectively. In the keV or lower energy range, the assumptions in the model breakdown, and the calculated incident-angle dependence, which agrees with the observed dependence [15] for angles of more than 60°, deviates from the inverse cosine law: at projectile energy E_p = 300 eV, $\sigma(60°)/\sigma(0)$ = 1.59 (calculation with a flat surface), and $\approx$ 1.6 (according to the experiment by Bronshtein and Dolinin [15]). The surface roughness influences the incident-angle dependence of the secondary electron emission in the following manner. One is the dispersion of incident angle to the microscopic boundary of the rough surface. This results in a relatively small increase in σ with increasing ϕ in comparison with that for the flat surface; e.g., $\sigma(60°)/\sigma(0)$ = 1.23 for H = 75 nm and W = 25 nm. The other is the blocking of the projectile electrons bombarding near the bottom of the roughness. This results in a suppression of the re-entrance of electrons in the case of oblique incidence, so that for large roughness (H/W > 10) the incident-angle dependence is enhanced (e.g., $\sigma(60°)/\sigma(0)$ = 1.92 for H = 750 nm and W = 25 nm).

Figure 20 shows the doubly differential yields $d^2\sigma/dE_s d\theta$ of electrons emitted in the forward (x < 0) and backward (x > 0) directions from a bowl-structured surface with obliquely incident electrons. A strong anisotropy between forward and backward directions is caused by the topographic feature of the surface. Because of dominant bombardment to an inclined plane ($2W \leq x \leq 4W$) of the surface, the number of secondary electrons emitted in the forward direction (x < 0) decreases, whereas it increases in the backward direction (x > 0). Also, the enhanced emission in the backward direction is accompanied with the low-energy shift of the energy distribution (due to emission of low-energy electrons from the inclined plane), as well as the large-angle emission (due to blocking of the projectile bombardment near the bottom of the surface).

In our model, the surface roughness is described in an oversimplified way by bowl-and-ripple structured surfaces and only the topographic effects on the secondary electron emission are discussed, in spite of possible changes in the surface work function as well as complicated topographies of plasma facing material surfaces. Furthermore, in any plasma, a plasma sheath develops. The plasma sheath may force "primary electrons" to bombard the surface perpendicular to the microscopic

Normal incidence

Oblique incidence on bowl surface
(H=75 nm, W=25 nm)
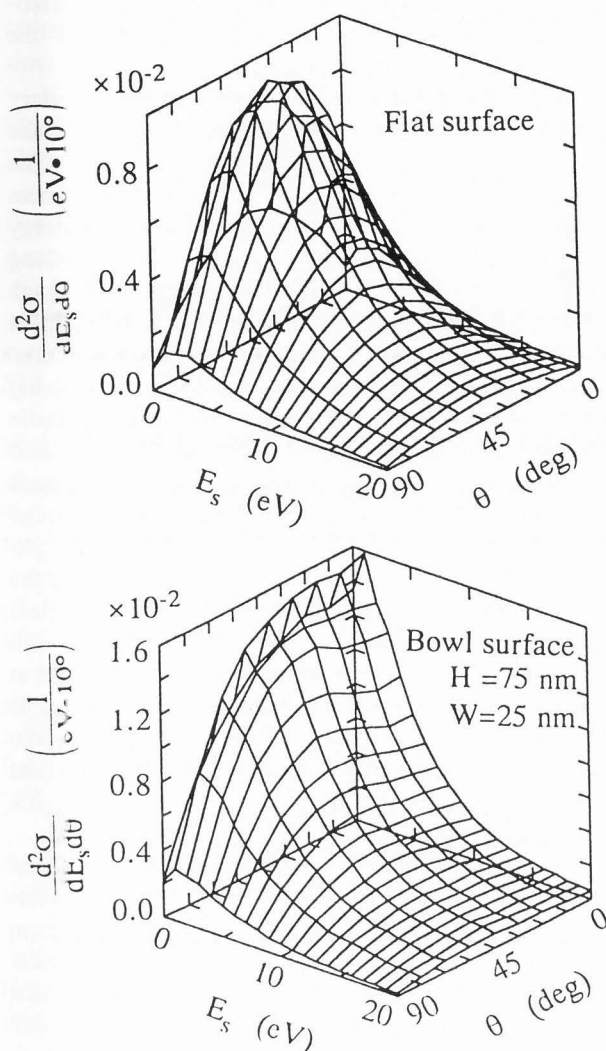
Figure 19. Doubly differential secondary electron yield $d^2\sigma/dE_s d\theta$ with respect to the energy E_s and polar angle θ of secondary electrons emitted from flat and bowl-structured surfaces for normal incidence of 300-eV electrons.
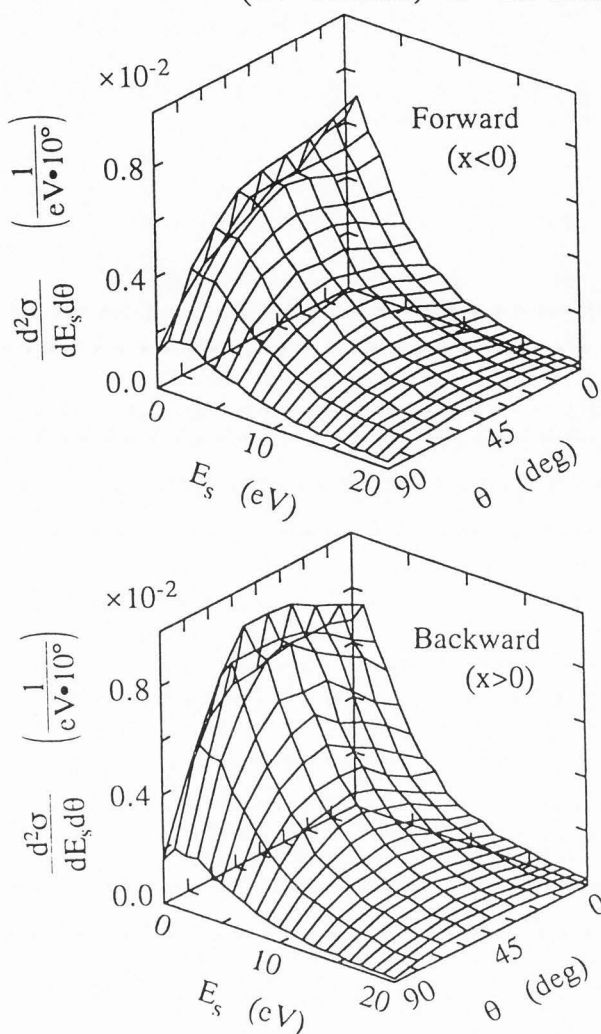
Figure 20. Doubly differential secondary electron yield $d^2\sigma/dE_s d\theta$ with respect to the energy E_s and polar angle θ of secondary electrons emitted in the forward direction (x < 0) and backward direction (x > 0), from a bowl-structured surface for oblique incidence ($\phi = 60°$) of 300-eV electrons.

roughness plane. The effects of the inclined surface and re-entrance will occur even in these real conditions because they are related mainly to the energy loss of "secondary electrons" in the solid and the topographic features of the surface, from which secondary electrons can escape. Nevertheless, due to fractal features or overlapping of many structures with different Ws and Hs, the two effects may not be clearly distinguishable from each other.

Conclusions

We have reported on our simulation models of kinetic electron emission from a metal surface due to ion bombardment as well as of secondary electron emission due to electron bombardment, and described theoretical treatments used for elastic and inelastic interactions of a projectile particle and excited electrons in the solid. Applications to beryllium, which is one of the candidate

materials for plasma facing components in thermonuclear fusion devices, reveal some interesting physics. The main points of our numerical simulation are as follows:

(1) We studied the electron emission under electron and proton bombardments at keV energy range by means of the Monte Carlo model. Due to the difference between the cross-sections for electronic excitation by primary electrons and by protons, the calculated electron yield by electron bombardment decreased with increasing impact energy, whereas an opposite trend was found for proton bombardment. Despite the opposite energy dependence of the electron yields, the energy distribution of electrons emitted from a beryllium surface by proton bombardment is similar to that by electron bombardment. The energy distribution peaked at an energy of about 3 eV and broadened towards high-energy side as the impact energy of electrons (protons) decreases (increases). The similarity of the energy distributions for electron and proton bombardments occurs because the majority of electrons emitted are produced through the electron cascade process in which each electron was excited by a projectile. Electrons emitted from the surface originate mainly within a depth of less than 40 Å, and the excitation depth of the electrons for proton bombardment is shallower than that for electron bombardment, dependant on the cross-section of electron excitations. With respect to the electron emission statistics, i.e., the probabilities W_n for emission of a given number n of electrons due to a single impact event, deviations from the Poisson distribution are seen: a larger W_0 and larger W_ns for high n emission (n $\geq$ 2). These deviations are explained with the backscattering of projectile particles and the cascade generation of electrons. The backscattering effect is small. Due to a larger energy transferred from a primary electron to a secondary electron, the electron cascade by electron bombardment develops extensively than that by proton bombardment, so that the emission statistics for electron bombardment deviates further from the Poisson distribution.

(2) The Monte Carlo model was applied to analyzing the effect of electron excitation by recoiling solid atoms, projectile charge state and projectile mass, and its threshold energy on the kinetic emission due to heavy-ion bombardment. To a first approximation of excitation of conduction electrons, the KE threshold energy (the electron yield) becomes higher (smaller) because of less energy transferred from a heavier ion to an electron for a given ion energy; the energy of emitted electrons is progressively lower as the ion gets heavier. With the increasing projectile initial charge state, the calculated electron yield becomes large; in this study, we only considered the excitation of conduction electrons by the ion. In the electron emission statistics, probabilities for emission decreases with the decreasing impact energy, al-

though potential emission mechanism produced electrons, even at a very low impact energy. The peak of the energy distribution (as well as the shape of distribution) of emitted electrons was independent of the charge state of the projectile.

(3) The Monte Carlo simulation of the secondary electron emission from beryllium was combined with the model of the bowl- and ripple-structured surfaces. The emphasis was placed on the effect of surface roughness on the secondary electron yield as well as on the energy and angular distribution of secondary electrons. As long as the primary electron is incident normal to the rough surface, the following two effects, due to topographic features of the surface, were demonstrated: (a) emission of low-energy electrons, from an inclined plane, which cannot escape from a flat surface due to inelastic energy loss in their transport to the surface, increases secondary electron yield and the low-energy component in the energy distribution; and (b) re-entrance of once-emitted electrons into the adjacent part of the topographic surface decreases the secondary electron yield and the number of electrons emitted with large oblique angles. As a result, the primary energy at which the maximum yield occurs is higher, and the decrease in the yield at the primary energies of more than the peak energy is lower than that for a flat surface. Furthermore, the shape of the energy distribution of secondary electrons shifted by 1-2 eV towards the low-energy side, a cosine distribution is obtained.

The similarity between secondary electron emissions for normal (incident angle $\phi = 0°$) and oblique incidences (incident angle ϕ) on a rough-textured beryllium is the small increase in σ with increasing ϕ; this results from the change in incident angle due to the surface topography. The difference is the blocking of primary electrons from bombarding near the bottom of the rough areas at oblique incidence; this results in a suppression of the re-entrance of electrons emitted at large angles into an adjacent part of the topographic surface. For oblique incidence, the number of secondary electrons emitted in the forward direction (as for example, the specular reflection of primary electrons) decreases, whereas, it increases in the backward direction. The secondary electron emission in the backward direction is accompanied with the low-energy shift of the energy distribution.

References

[1] Akkerman AF, Chernov GYa (1978). Mean free paths by inelastic interactions, stopping powers, and energy straggling for electrons of energies up to 20 keV in various solids. phys. stat. sol. **B89**, 329-333.

[2] Alonso EV, Baragiola RA, Ferrón J, Jakas MM, Oliva-Florio A (1980). Z_1 dependence of ion-induced

electron emission from aluminum. Phys. Rev. **B22**, 80-87.

[3] Alonso EV, Alurralde MA, Baragiola RA (1986). Kinetic electron emission from solids induced by slow heavy ions. Surf. Sci. **166**, L155-L160.

[4] Asselt WK van, Poelsema B, Boers AL (1978). Electron back-scattering in a surface-barrier detector. J. Phys. D: Appl. Phys. **11**, L107-L110.

[5] Auciello O, Kelly R (eds.) (1984). Ion Bombardment Modification of Surfaces. Elsevier, Amsterdam. pp. 1-466.

[6] Aumayr F, Winter H (1994). Electron emission induced by slow highly charged ions on a clean metal surface. Nucl. Instrum. Methods Phys. Res. **B90**, 523-532.

[7] Azuma T, Yamazaki Y, Komaki K, Sekiguchi M, Hasegawa T, Hattori T, Kuroki K (1992). Secondary electron emission from a C-foil resulting from the passage of orientation selected He^{2+} molecular ions. Nucl. Instrum. Methods Phys. Res. **B67**, 636-640.

[8] Baragiola RA (1993). Principles and mechanisms of ion induced electron emission. Nucl. Instrum. Methods Phys. Res. **B78**, 223-238.

[9] Baragiola RA (1994). Electron emission from slow ion-solid interactions. In: Low energy ion-surface interactions. Wiley Series in Ion Chemistry and Physics. Rabalais JW (ed.). John Wiley & Sons, New York. pp. 187-262.

[10] Baragiola RA, Alonso EV, Oliva A, Bonanno A, Xu F (1992). Fast electrons from slow atomic collisions. Phys. Rev. **A45**, 5286-5288.

[11] Benka O, Steinbauer E, Bolik O, Fink T (1994). Statistics of electron emission induced by MeV H^+ and He^+ ions. Nucl. Instrum. Methods Phys. Res. **B93**, 156-160.

[12] Beuhler RJ, Friedman L (1977). Low noise, high voltage secondary emission ion detector for polyatomic ions. Int. J. Mass Spectrom. Ion Phys. **23**, 81-97.

[13] Biersack JP, Eckstein W (1984). Sputtering studies with the Monte Carlo program TRIM.SP. Appl. Phys. **A34**, 73-94.

[14] Biersack JP, Haggmark LG (1980). A Monte Carlo computer program for the transport of energetic ions in amorphous targets. Nucl. Instrum. Methods, **174**, 257-269.

[15] Bronshtein IM, Dolinin VA (1968). The secondary electron emission (SEE) of solids at large angles of incidence of the primary beam. Sov. Phys. - Solid State. **9**, 2133-2140.

[16] Brooks JN (1980). Self-consistent calculations of edge temperature and self-sputtering of the limiter surface for tokamak fusion reactors. J. Nucl. Mater. **93/94**, 437-441.

[17] Cailler M, Ganachaud JP (1990). Secondary electron emission from solids. II. Theoretical descriptions. Scanning Microsc. Suppl. **4**, 81-110.

[18] Darlington EH (1975). Backscattering of 10-100 keV electrons from thick targets. J. Phys. D: Appl. Phys. **8**, 85-93.

[19] Delaney CFG, Walton PW (1966). Measurement of the statistics of secondary electron emission. IEEE Trans. Nucl. Sci. **NS-13**, 742-751.

[20] Dubus A, Dehaes J-C, Ganachaud JP, Hafni A, Cailler M (1993). Monte Carlo evaluation of the influence of the interaction cross-sections on the secondary-electron-emission yields from polycrystalline aluminum targets. Phys. Rev. **B47**, 11056-11073.

[21] Eckstein W (1991). Computer Simulation of Ion-Solid Interactions. Springer Series in Materials Science 10. Springer-Verlag, Berlin. pp. 4-32.

[22] Eckstein W, Mashkova ES, Molchanov VA, Sidorov AV, Zhukova YuN (1993). The effect of target texture and topography on the spatial distribution of material sputtered from tungsten. Appl. Phys. **A57**, 271-277.

[23] Fitting HJ (1974). Transmission, energy distribution, and SE excitation of fast electrons in thin solid films. phys. stat. sol. **A26**, 525-535.

[24] Fitting H-J, Reinhardt J (1985). Monte-Carlo simulation of keV-electron scattering in solids targets. phys. stat. sol. **A88**, 245-259.

[25] Forman R (1978). Secondary electron emission properties of conducting surfaces for use in multi-stage depressed collectors. IEEE Trans. Electron Devices **ED-25**, 69-70.

[26] Ganachaud JP, Cailler M (1979). A Monte-Carlo calculation of the secondary electron emission of normal metals. I. The model. Surf. Sci. **83**, 498-518.

[27] Gryzinski M (1965). Classical theory of atomic collisions. I. Theory of inelastic collisions. Phys. Rev. **A138**, 336-358.

[28] Hasselkamp D, Scharmann A (1983). Die Sekundärelektronenemission von Aluminum beim Beschuß mit H^+-, He^+-, Ne^+- und Ar^+-Ionen im Energiebereich von 100 keV bis 800 keV: Teil II (Secondary electron emission from aluminum under bombardment by H^+-, He^+-, Ne^+- and Ar^+-ions in the energy range 100 keV to 800 keV: Part II). Vak.-Tech. **32**, 9-16.

[29] Hasselkamp D, Hippler S, Scharmann A (1987). Ion-induced secondary electron spectra from clean metal surfaces. Nucl. Instrum. Methods Phys. Res. **B18**, 561-565.

[30] Hasselkamp D, Hippler S, Scharmann A, Schmehl T (1990). Electron emission from clean solid surfaces by fast ions. Ann. Phys. (Leipzig) **47**, 555-567.

[31] Hasselkamp D, Rothard H, Groeneveld K-O, Kemmler J, Varga P, Winter H (1992). Particle Induced

Electron Emission II. Springer Tracts in Modern Physics 123. Springer-Verlag, Berlin. pp. 1-220, and references therein.

[32] Hofer WO (1987). Plasma-surface interactions: The role of charged particle emission. J. Vac. Sci. Thechnol. **A5**, 2213-2216.

[33] Hofer WO (1990). Ion-induced electron emission from solids. Scanning Microsc. Suppl. **4**, 265-310.

[34] Jablonski A, Gryko J, Kraaer J, Tougaard S (1989). Elastic electron backscttering from surfaces. Phys. Rev. **B39**, 61-71.

[35] Kawata J, Ohya K (1994). Surface roughness effect on secondary electron emission from beryllium under electron bombardment. J. Phys. Soc. Jpn. **63**, 795-806.

[36] Kawata J, Ohya K (1995). Contribution of kinetic emission to multi-charged ion-induced electron emission from a metal surface. Nucl. Instrum. Methods Phys. Res. **B98**, 450-453.

[37] Kawata J, Ohya K, Mori I (1991). Influence of recoiling target atoms on kinetic electron emission from molybdenum under keV ion bombardments. Jpn. J. Appl. Phys. **30**, 2585-2591.

[38] Koborov NN, Kurnaev VA, Sotnikov VM (1984). The surface roughness influence on the light ions backscattering. J. Nucl. Mater. **128/129**, 691-693.

[39] Komaki K (1991). Number distribution of multiply emitted secondary electrons (MUSE) produced by atomic and molecular ion impacts on thin foils. Radiat. Eff. Defects Solids **117**, 125 (extended abstract).

[40] Koshikawa T, Shimizu R (1974). A Monte Carlo calculation of low-energy secondary electron emission from metals. J. Phys. D: Appl. Phys. **7**, 1303-1315.

[41] Koshikawa T, Goto K, Shimizu R, Ishikawa K (1974). Secondary electron energy spectra from a Be layer evaporated on Cu. J. Phys. D: Appl. Phys. **7**, L174-L177.

[42] Kotera M, Ijichi R, Fujiwara T, Suga H, Wittry DB (1990). A simulation of electron scattering in metals. Jpn. J. Appl. Phys. **29**, 2277-2282.

[43] Kozochkina AA, Leonas VB, Witte M (1991). Probabilities of multiple electron emission from thin ($\sim$ 50 Å) carbon foils after impact of neutral oxygen at energies between 30 and 200 keV. Nucl. Instrum. Methods Phys. Res. **B62**, 51-57.

[44] Lakits G, Aumayr F, Winter H (1989). On the statistics of heavy-particle-induced kinetic electron emission from a clean metal surface. Phys. Lett. **A139**, 395-398.

[45] Lakits G, Aumayr F, Heim M, Winter H (1990). Threshold of ion-induced kinetic electron emission from a clean metal surface. Phys. Rev. **A42**, 5780-5783.

[46] Lakits G, Arnau A, Winter H (1990). Slow-particle-induced kinetic electron emission from a clean metal surface: A comparison for neutral and ionized projectiles. Phys. Rev. **B42**, 15-24.

[47] Lindhard J (1954). On the properties of a gas of charged particles. Kgl. Danske Videnskab Selskab Mat. Fys. Medd. **28**, 1-57.

[48] Littmark U, Hofer WO (1978). The influence of surface structures on sputtering: Angular distribution and yield from faceted surfaces. J. Mater. Sci. **13**, 2577-2586.

[49] Mandrekas J, Singer CE, Ruzic DN (1987). Effects of the plasma-wall sheath on transport. J. Vac. Sci. Technol. **A5**, 2315-2318.

[50] Oda K, Kanie T, Ichimiya A, Ohtani S, Ohya K, Tawara H (1992). Secondary electron emission from a clean tantalum surface under keV rare gas neutral beam bombardment. Surf. Sci. **262**, 437-443.

[51] Ohya K, Kawata J, Mori I (1991). Elastic scattering cross sections of low-energy electron in solids. Jpn. J. Appl. Phys. **30**, 2611-2612.

[52] Ohya K, Aumayr F, Winter H (1992). Statistics of ion-induced kinetic electron emission: A comparison between experimental and Monte Carlo-simulated results. Phys. Rev. **B46**, 3101-3104.

[53] Ono S, Kanaya K (1979). The energy dependence of secondary emission based on range-energy retardation power formula. J. Phys. D: Appl. Phys. **12**, 619-632.

[54] Ploch W (1951). Mässenabhangigkeit der Elektronenauslösung durch isotope Ionen (Mass dependence of electron emission with isotope ions). Z. Physik, **130**, 174-195.

[55] Raether H (1980). Excitation of Plasmons and Interband Transitions by Electrons. Springer Tracts in Modern Physics 88. Springer-Verlag, Berlin. p. 10-12.

[56] Rösler M (1994). Plasmon effects in the particle-induced kinetic electron emission from nearly-free-electron metals. Nucl. Instrum. Methods Phys. Res. **B90**, 537-541.

[57] Rösler M, Brauer W, Devooght J, Dehaes J-C, Dubus A, Cailler M, Ganachaud JP (1991). Particle Induced Electron Emission I. Springer Tracts in Modern Physics 122. Springer-Verlag, Berlin. pp. 1-130, and references therein.

[58] Ruzic DN (1990). The effects of surface roughness characterized by fractal geometry on sputtering. Nucl. Instrum. Methods Phys. Res. **B47**, 118-125.

[59] Schmid R, Gaukler KH, Seiler H (1983). Measurement of elastically reflected electrons ($E \leq 2.5$ keV) for imaging of surfaces in a simple ultra high vacuum scanning electron microscope. Scanning Electron Microsc. **1983**; II, 501-509.

[60] Schou J (1988). Secondary electron emission

from solids by electron and proton bombardment. Scanning Microsc. **2**, 607-632.

[61] Seah MP, Dench WA (1979). Quantitative electron spectroscopy of surfaces: A standard data base for electron inelastic mean free path. Surf. Interface Anal. **1**, 2-11.

[62] Seiler H (1967). Einige aktuelle Probleme der Sekundärelektronenemission (Some recent problems related to secondary electron emission). Z. Angew. Phys. **22**, 249-263.

[63] Shimizu R, Kataoka Y, Ikuta T, Koshikawa T, Hashimoto H (1976). A Monte Carlo approach to the direct simulation of electron penetration in solids. J. Phys. D: Appl. Phys. **9**, 101-114.

[64] Shorin VS, Sosnin AN (1991). The shape of the ion backscattering spectrum for a surface having sine wave relief. Nucl. Instrum. Methods Phys. Res. **B53**, 199-201.

[65] Smidts C, Dubus A, Dehaes JC, Hafni A, Ganachaud JP (1992). Study of the influence of the electron capture and loss process on the secondary electron emission induced by protons in aluminum. Nucl. Instrum. Methods Phys. Res. **B67**, 646-649.

[66] Stangeby PC, McCracken GM (1990). Plasma boundary phenomena in tokamaks. Nucl. Fusion **30**, 1225-1379, and references therein.

[67] Sternglass EJ (1957). Theory of secondary electron emission by high-speed ions. Phys. Rev. **108**, 1-12.

[68] Suleman M, Pattinson EB (1980). The SEE yield changes in slowly oxidised Be with surface characterisation by AES. J. Phys. D: Appl. Phys. **13**, 693-700.

[69] Tanabe T, Noda N, Nakamura H (1992). Review of high Z materials for PSI applications. J. Nucl. Mater. **196-198**, 11-27.

[70] Thomas EW (1991). Particle induced electron emission. In: Atomic and Plasma-Material Interaction Data for Fusion. Suppl. Nucl. Fusion, Vol. 1. Janev RK (ed.). International Atomic Energy Agency, Vienna, Austria. pp. 79-91.

[71] Thomas PR and the JET team (1990). Results of JET operation with beryllium. J. Nucl. Mater. **176/177**, 3-13.

[72] Tung CJ, Ritchie RH (1977). Electron slowing-down spectra in aluminum metal. Phys. Rev. **B16**, 4302-4313.

[73] Utsumi K, Ichimaru S (1982). Dielectric formulation of strongly coupled electron liquids at metallic densities. VI. Analytic expression for the local-field correction. Phys. Rev. **A26**, 603-610.

[74] Vana M, Kurz H, Winter HP, Aumayr F (1995). Potential and kinetic electron emission from clean gold induced by multi-charged nitrogen ions. Nucl. Instrum. Methods Phys. Res. **B100**, 402-406.

[75] Wang Y-N, Ma TC (1990). Stopping power and energy-loss straggling of slow protons in a strongly coupled degenerate electron gas. Nucl. Instrum. Methods Phys. Res. **B51**, 216-218.

[76] Wang Y-N, Ma TC (1993). Numerical evaluation of the electronic stopping power for heavy ions in solids. Nucl. Instrum. Methods Phys. Res. **B80/B81**, 16-19.

[77] Winter H, Aumayr F, Lakits G (1991). Recent advances in understanding particle-induced electron emission from metal surfaces. Nucl. Instrum. Methods Phys. Res. **B58**, 301-308.

[78] Wüest M, Bochsler P (1992). Simulation of ion backscattering from rough surfaces. Nucl. Instrum. Methods Phys. Res. **B71**, 314-323.

[79] Ziegler JF, Biersack JP, Littmark U (1985). The Stopping and Range of Ions in Solids. The Stopping and Range of Ions in Matter, Vol.1. Ziegler JF (ed.). Pergamon Press, New York. pp. 66-140, and references therein.

[80] Yamamura Y, Mössner C, Oechsner H (1987). The bombarding-angle dependence of sputtering yields under various surface conditions. Radiat. Eff. **103**, 25-43.

Discussions with Reviewers

W.O. Hofer: What is the physical meaning of the word "direct" in the direct Monte Carlo simulation?
Authors: Conventional Monte Carlo simulation derives the average rate of the energy loss of a particle from the electronic stopping power on the basis of a continuous slowing-down approximation. One can properly talk of "direct simulation" when incorporating differential cross-sections for each of the inelastic processes, e.g., conduction electron, plasmon and inner-shell electron excitations (that one hope to represent more or less correctly the true physical process). Therefore, we use the word "direct Monte Carlo simulation" for secondary electron emission by electron bombardment.

D. Hasselkamp: You have applied the simulation method to beryllium, are the results typical also for other metals?
Authors: We have applied our simulation model not only to beryllium and aluminum, but also to gold which is not a nearly-free-electron metal but a transition metal. The calculated electron emission statistics of gold, by impact of protons, reproduce the observed deviation from the Poisson distribution, which is larger than that of beryllium, due to larger backscattering of projectile ions [83]. Furthermore, the calculated electron yield and electron energy distribution are reasonable.

D. Hasselkamp: Plasmon decay leads to an observable shoulder in the energy spectra of Mg and Al. Why is no comparable structure visible in your calculations for Be?

Authors: In our simulation, bulk plasmons are not directly excited by a projectile ion, but they are excited in the electron cascade process as well as by a projectile electron. The large angle scattering of a projectile particle in Be is rare in comparison with Mg and Al, according to differential collision cross-section of elastic collision with ionic cores [51, 84]. This causes a longer range of the projectile in Be and a deeper excitation of electrons by the projectile, so that the electrons excited by a plasmon decay lose more energy through inelastic interactions in the solid. As a result, there is no shoulder in the energy distribution, but the plasmon decay causes both high-energy shift of the peak position and broadening of its shape.

D. Hasselkamp: Is there a simple relationship between the electron yields for proton impact and the corresponding inelastic energy loss at energies below 10 keV?

R. Baragiola: How do the authors describe the ion-induced electron emission from the calculation of the electronic stopping power?

Authors: The ratio between the calculated electron yield and the electronic stopping power becomes small as the impact energy is decreased at keV range. This is due to small energy transferred from a projectile ion to an electron, so that we no longer have the well-defined cascade multiplication of electrons, which can escape from the surface potential barrier. Therefore, the relationship between electron yield and the inelastic energy loss may be complicated and we have no explicit expression, although at higher impact energies, where the electron cascade is fully developed, the electron yield tends to be proportional to the electronic stopping power.

J. Schou: What is the reason that the calculated stopping power in Figure 3 is much less than that from the Ziegler-Biersack-Littmark formula?

Authors: The deviation at energies less than 100 eV may be due to strongly coupled correlation-exchange interactions of electron gas, as Valdés et al. [85] calculated more exactly. The lowest energies available for the ZBL compilation are about 10 keV and the ZBL formula used here is extrapolated down to much smaller energies, i.e., 10 eV, assuming velocity-proportional dependence {or (velocity)$^{0.5}$-proportional in Be}. For energies below a few keV the Oen-Robinson stopping power is the better choice according to range and variance calculation using TRIM.SP code [82], and the stopping power deviates from the ZBL extrapolation in the same manner as our calculated one [81].

J. Schou: The authors have made an interesting model for surface roughness and studied the influence on the yield, the energy spectra and the angular distribution. What happens if features of other shapes, e.g. (sharp) cones, cover the surface? Another point is that one may expect to have a distribution of surfaces features of different size present at the same time. What would be the result of such an inhomogeneous distribution of features for the yield and spectra?

Authors: The sharp-cone shaped surface structure may be analogous to our calculations for large aspect ratio of the roughness. In this case, due to dominant effect of re-entrance, the calculated electron yield becomes smaller than that for a flat surface. Secondary electrons are mostly emitted near the top of the roughness, where the effect of the inclined surface is dominant, as a result, the low-energy shift of the energy distribution and the large angle emission as well as the peak of small angle will be obtained. Even if other shapes or any distribution of surface features of different sizes are present, the topological effect of the roughness discussed here, almost only depends on H/W or the slope of the inclined plane as long as the range of the projectile particle or the escape depth of secondary electrons is smaller than the roughness. Therefore, the average H/W may be an important factor for evaluating the electron yield, the energy and angular distribution of emitted electrons.

R. Baragiola: Is there a kinetic energy threshold in the model for kinetic electron emission for ions?

Authors: A free-electron gas model of the conduction band is in this study used to obtain single electron excitation by a projectile ion, therefore, the calculated KE yield vanishes at the conventional threshold calculated from a head-on collision of the projectile ion with an electron, as described in the text. We are aware that, at low impact energies of keV or less, other electron-excitation mechanisms, e.g., electron promotion by heavy projectiles, will be dominant to the kinetic emission. Our tentative and approximate KE model, due to the electron promotion, produces KE at much lower energies than the conventional threshold [36].

H.-J. Fitting: You have used plasmon dispersion, but how did you weigh the cross-section for excitation of $\hbar\omega_p(q = 0)$ up to the cut-off value $\hbar\omega_p(q_c)$?

Authors: A simple Drude dielectric function [72] is used for the excitation of bulk plasmons with the energies from $\hbar\omega_p(q = 0)$ to $\hbar\omega_p(q_c)$, together with the plasmon dispersion relation. Although the Drude function includes the plasmon damping effect and gives an excitation of the plasmons with the energies less than $\hbar\omega_p(q = 0)$, we cut off the excitation at $\hbar\omega_p(q = 0)$ in our study.

H.-J. Fitting: The agreement of calculated and experimentally obtained backscattering fractions is a necessary quality proof of the Monte Carlo program used. There are still some deviations in Figure 5 between your calculated $\eta(E_p)$ values and the measured ones of Bronshtein. What is the reason for these deviations?

Authors: In this study, the elastic scattering angle (as well as the elastic mean free path) of a primary electron is evaluated using the screened Rutherford formula. The formula does not produce any oscillatory features in the differential cross-section at energies less than 100 eV and gives stronger scattering with large angles in comparison with the PWE (partial wave expansion) cross-section with the solid state potential for light materials [51]. It seems that the no-oscillatory feature causes no hump in $\eta(E_p < 500$ eV), whereas the large angle scattering causes larger η. Nevertheless, as reasons for the deviations, one may point out the effect of surface roughness that we have discussed, as well as change in the work function due to the surface contaminations.

M. Rösler: Normally, the excitation of conduction electrons by charged particles at normal incidence is predominantly directed in the inward direction. Therefore, the contribution of directly emitted electrons is less than 10% of the contribution determined by the electron cascade. What is the reason for the distinct higher ratio obtained from your calculation (Fig. 6)?

Authors: The excitation energy of an electron by a proton (i.e., the energy transfer from a proton to an electron) is much smaller than that by a primary electron, therefore, the cascade multiplication of the electron is insufficiently developed. This leads to small electron yield due to proton impact in keV energy range and large contribution of direct emitted electrons: e.g., at $E_p = 3$ keV, 0.163 and 34.6%, respectively, as shown in Figure 6. Furthermore, even due to impact of primary electron, the direct contribution largely depends on the primary energy: 22.4% and 9.4% at $E_p = 300$ eV and 3 keV, respectively. The large direct contribution at low energies results from the fact that the primary electrons are randomly directed near the surface due to frequent large-angle elastic scatterings, in addition to the insufficient development of the electron cascade.

M. Rösler: In your calculation, the elastic mean free path (MFP) obtained from the fit formula given in [24] was used. A more reliable MFP can be determined by a phase shift analysis. This leads to a lowering of the elastic MFP at low energies {obtained from unpublished results for the phase shifts calculated by K. Heinz (Erlangen) and also probably with your own program used in ref. [51]}. What are the consequences of such a behavior on the energy distribution of emitted electrons at low energies?

Authors: Our calculated PWE (partial wave expansion) MFP is smaller than the fit formula used in this simulation at low energies and it has a minimum value (≈ 2 Å) near 20 eV; with further decreasing energy, the MFP approaches the formula. The use of the PWE MFP in the transport process of secondary electrons leads to low-energy shift (≈ 1 eV) of the energy distribution of emitted electrons, which may result in better agreement with the observed distribution in Figure 7. However, the PWE MFP leads to considerably smaller electron yields (e.g., 0.381 at $E_p = 300$ eV) in comparison with the observed yield (Fig. 5). These are caused by the smaller MFPs of low-energy secondary electrons producing frequent elastic scatterings and then strong inelastic energy loss during their transport to the surface; this causes the lowering of the electron escape depth.

Additional References

[81] Eckstein W (1991). Computer Simulation of Ion-Solid Interactions. Springer Series in Materials Science 10. Springer-Verlag, Berlin. pp. 63-72.

[82] Mayer M, Eckstein W (1994). Monte Carlo calculations of hydrogen and deuterium range distributions in light target materials. Nucl. Instrum. Methods Phys. Res. **B94**, 22-26.

[83] Ohya K, Kawata J (1993). Direct Monte Carlo simulation of ion-induced kinetic electron emission statistics. Jpn. J. Appl. Phys. **32**, 1803-1807.

[84] Ohya K, Kawata J, Mori I (1992). Partial wave expansion of ion-atom elastic scattering in solids. Nucl. Instrum. Methods Phys. Res. **B67**, 419-422.

[85] Valdés JE, Eckardt JC, Lantschner GH, Arista NR (1994). Energy loss of slow protons in solids: Deviation from the proportionality with projectile velocity. Phys. Rev. **A49**, 1083-1088.